frontiers in Earth Science

ORIGINAL RESEARCH
published: 15 April 2020
doi: 10.3389/feart.2020.00097

Limb-Bone Development of Seymouriamorphs: Implications for the Evolution of Growth Strategy in Stem Amniotes

Jordi Estefa[1], Jozef Klembara[2], Paul Tafforeau[3] and Sophie Sanchez[1,3]**

[1] Subdepartment of Evolution and Development, Evolutionary Biology Center, Department of Organismal Biology, Uppsala University, Uppsala, Sweden, [2] Department of Ecology, Faculty of Natural Sciences, Comenius University in Bratislava, Bratislava, Slovakia, [3] European Synchrotron Radiation Facility, Grenoble, France

OPEN ACCESS

Edited by:
Michel Laurin,
UMR 7207 Centre de Recherche sur la Paléobiodiversité et les Paléoenvironnements (CR2P), France

Reviewed by:
Holly Woodward,
Oklahoma State University Center for Health Sciences, United States
Graciela Helena Piñeiro,
Universidad de la República, Uruguay
Vivian De Buffrénil,
Muséum National d'Histoire Naturelle, France

***Correspondence:**
Jordi Estefa
jordi.estefa@ebc.uu.se
Sophie Sanchez
sophie.sanchez@ebc.uu.se

Specialty section:
This article was submitted to Paleontology, a section of the journal Frontiers in Earth Science

Received: 17 July 2019
Accepted: 20 March 2020
Published: 15 April 2020

Citation:
Estefa J, Klembara J, Tafforeau P and Sanchez S (2020) Limb-Bone Development of Seymouriamorphs: Implications for the Evolution of Growth Strategy in Stem Amniotes. Front. Earth Sci. 8:97. doi: 10.3389/feart.2020.00097

Tetrapod life on land was the result of a lengthy process, the final steps of which resulted in full independence of amniotic tetrapods from the aquatic environment. Developmental strategies, including growth rate and the attainment of sexual maturity, played a major role in this transition. Early amniotes, such as *Ophiacodon*, tended to reach sexual maturity in a year while most non-amniotic Paleozoic tetrapods (including Devonian tetrapods and temnospondyls) became adult after 3 to 11 years. This ontogenetic transition is accompanied by a drastic change in growth rate and bone microstructure suggesting faster growth dynamics in early amniotes than in Devonian tetrapods and temnospondyls. Was the acquisition of a faster development (earlier sexual maturity and faster growth rate) a drastic evolutionary event or an extended process over geological time? To answer this question, the limb bone histology of two Early Permian (i.e., 270–290 million-year-old) stem-amniote seymouriamorphs, *Seymouria sanjuanensis* and *Discosauriscus austriacus*, were investigated. We used three-dimensional bone paleohistology based on propagation phase-contrast synchrotron microtomography. Both seymouriamorphs display relatively fast bone growth and dynamics (even though cyclic in the humerus of *D. austriacus*). This significantly contrasts with the slow primary bone deposition encountered in the stylopods of temnospondyls and Devonian (i.e., 360 million-year-old) stem tetrapods of similar sizes. On the basis of skeletochronological data, the seymouriamorph *D. austriacus* retained a long pre-reproductive period as observed in Devonian tetrapods and most temnospondyls. The combination of characteristics (faster growth rate but long pre-reproductive period) suggests that the shift toward an amniotic developmental strategy was an extended process in the evolutionary history of amniotes.

Keywords: life history, early tetrapods, synchrotron imaging, three-dimensional paleohistology, cortical microstructure

INTRODUCTION

Amniotes were the first animals in the evolutionary history of vertebrates to become independent from the aquatic environment (Sumida and Martin, 1997; Sander, 2012). This ecological transition not only resulted in the evolution of an amniotic egg (Reisz, 1997; Piñeiro et al., 2012) but significantly affected the life history traits of amniotes, including reproductive strategies (i.e., live-bearing versus egg lay-down, Piñeiro et al., 2012; Sander, 2012; egg number and size, Duellman and Trueb, 1994; parental care, Crump, 1996; Botha-Brink and Modesto, 2007; Rafferty and Reina, 2012), skeletal maturity and growth rate (Sanchez et al., 2008). Was this overall transition (i.e., life history and reproduction) a gradual process or a single drastic evolutionary event? Paleontologists have put considerable effort into investigating the evolution of new reproductive strategies in stem amniotes (Botha-Brink and Modesto, 2007; Piñeiro et al., 2012; Sander, 2012) but the skeletal life-history data bearing on this transition have received little attention. We focus here on the skeletal maturity and bone growth rate of stem amniotes.

The first amniotes appeared during the late Paleozoic, a little more than 300 million years ago. A recent skeletochronological study revealed that the skeletal development of the basal synapsid *Ophiacodon* (Benson, 2012) drastically slowed down after a year (Laurin and de Buffrénil, 2016) while most non-amniotic tetrapods from the Paleozoic tend to slow down their growth after several years (e.g., Sanchez et al., 2008, 2014, 2016; Kamska et al., 2019). Histological investigations demonstrated that Devonian (i.e., 380–360 million-year-old) stem tetrapods had a slow development with a late onset of sexual maturity and a slow growth rate (Sanchez et al., 2014, 2016; Kamska et al., 2019) compared to early amniotes of the same size (e.g., *Ophiacodon*, Laurin and de Buffrénil, 2016). This would suggest that the emergence of amniotes could be characterized by an earlier onset of sexual maturity and a faster bone-growth rate. In order to investigate this shift in skeletal development and bone dynamics, we decided to focus on seymouriamorphs, considered by most authors as stem amniotes (e.g., Anderson, 2007, 2008; Ruta and Coates, 2007; Sigurdsen and Green, 2011; Pardo et al., 2017a – even though a diverging opinion has been published, Vallin and Laurin, 2004; Marjanović and Laurin, 2013 – see phylogenetic considerations in Section "Materials and Methods").

We decided to focus on the long-bone histology. Long bones comprise a cylinder of cortical bone surrounding a marrow cavity which can be filled in by trabeculae. The cortical bone displays, in most tetrapods, an incremental growth pattern (Castanet et al., 1993; Woodward et al., 2014) which reflects cyclical bone deposition (Castanet et al., 1993; Köhler et al., 2012; Padian, 2012). This pattern is often preserved during fossilization (e.g., Steyer et al., 2004; Erickson, 2005; de Ricqlès et al., 2006; Sanchez et al., 2008). Certain life-history traits such as somatic age, ontogenetic stage and growth strategy can therefore be (partly) retrieved from the bone record of fossil long bones, depending on their degree of osteoclast-mediated erosion and/or remodeling intensity (Castanet et al., 1993).

Sanchez et al. (2008) already suggested that *Discosauriscus austriacus*, although a stem amniote according to the prevailing phylogenetic hypothesis (**Figure 1**), retained primitive developmental and skeletal features such as a long-lasting juvenile stage and a slow bone growth rate. We have decided to enlarge our sampling to another stem amniote, *Seymouria sanjuanensis* (**Figure 1**). The limb-bone histology of *S. sanjuanensis* has never been addressed (only their ribs and dermal bones were investigated; de Ricqlès, 1981). Because the specimen of *S. sanjuanensis* could not be sectioned, we used a non-destructive three-dimensional (3D) imaging technique: Propagation Phase-Contrast Synchrotron Radiation Micro-Computed Tomography (PPC-SRμCT). This tool was originally developed for virtual dental paleohistology (Tafforeau and Smith, 2008; Tafforeau et al., 2012) and later adapted to fossil bones (Sanchez et al., 2012, 2013, 2016). For comparative reasons, we have re-examined the long bones of *D. austriacus* using the same methods.

MATERIALS AND METHODS

Material – Taxa Studied

Discosauriscus austriacus is known from the Lower Permian (290 My) of Western and Central Europe (Klembara and Meszároš, 1992). Hundreds of specimens were found in bituminous shales suggesting a lacustrine environment. They were associated with remnants of actinopterygians and chondrichthyans (Klembara and Meszároš, 1992). The skull-roof bones of most individuals considered as juveniles (Sanchez et al., 2008) exhibit sensory grooves. They host neuromast cells innervated by the cranial nerves to help the animals detect movements of prey and predators in the aquatic environment. *D. austriacus* has been considered amphibious until the late juvenile stage (Klembara et al., 2001; Sanchez et al., 2008). The largest specimen (SNM Z

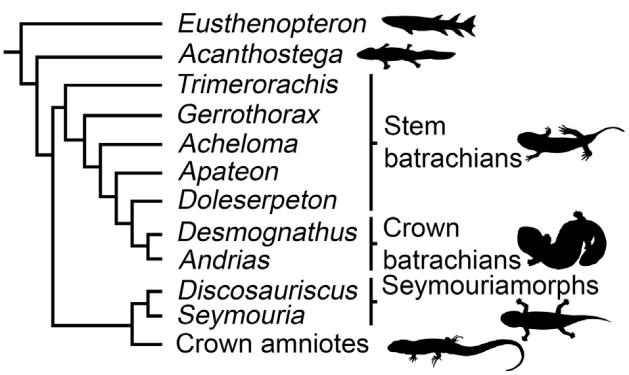

FIGURE 1 | Phylogenetic relationships of the studied species (based on Ruta and Coates, 2007; Ruta et al., 2007; Pardo et al., 2017a,b). Silhouettes: *Eusthenopteron* modified from Nobu Tamura (https://creativecommons.org/licenses/by/2.5/); *Acanthostega* by Nobu Tamura (https://creativecommons.org/licenses/by-sa/3.0/); Stem batrachians by Scott Hartman (http://creativecommons.org/licenses/by/3.0/); Crown batrachians by Y. de Hoev and vectorized by T. Michael Keesey (Public domain); Seymouriamorphs by Nobu Tamura and vectorized by T. Michael Keesey (https://creativecommons.org/licenses/by-sa/3.0/); Crown amniotes (Public domain).

25814) however lacks these sensory grooves and may, for this reason, as well as other anatomical characteristics, represent a terrestrial adult (Klembara, 2009). The specimen SNM Z 25814 was about 40 cm long including the tail (with a skull length estimated to 6.2 cm; Klembara, 1995). The terrestrial lifestyle of adult specimens of *D. austriacus* has been confirmed by another study based on limb bone compactness (Kriloff et al., 2008).

Seymouria sanjuanensis is one of these terrestrial presumed stem amniotes that widely spread along the central Pangean mountains during the Early Permian (270–280 My). It was first described from the Wolfcampian horizon of the Cutler Formation in the south-east of Utah, United States (Vaughn, 1966). A few specimens were later discovered in the Upper Cutler Formation of New Mexico (Berman et al., 1987), and in the Tambach Formation of Central Germany (Berman and Martens, 1993; Berman et al., 2000). Individuals were about 60 cm long (including the tail) at the adult stage (Berman et al., 2000). The skull roof bones of both the juvenile and adult individuals lack sensory grooves (Klembara et al., 2007), suggesting that both juveniles and adults were substantially independent of the aquatic environment (White, 1939; Berman and Martens, 1993) except for the reproduction and larval period. Multiple pronounced muscular scars on the skeleton indicate a strong musculature able to support the weight of the animal on land. The dentition of *Seymouria* suggests a generalist carnivorous diet (White, 1939).

Material – Phylogenetic Considerations

Initially *S. sanjuanensis* and *D. austriacus* were regarded as "primitive reptiles" (Romer, 1928; White, 1939). So far, no consensus has been found on the phylogeny of early tetrapods. The controversy lies in the ongoing debate about the origin of crown amphibians, i.e., urodeles (salamanders), anurans (frogs), and caecilians (Milner, 1988; Trueb and Cloutier, 1991; Schoch and Milner, 2004; Vallin and Laurin, 2004; Ruta and Coates, 2007; Anderson, 2008; Sigurdsen and Green, 2011; Marjanović and Laurin, 2013; Pardo et al., 2017a; Schoch, 2018). If batrachians (including frogs and salamanders) originated within branchiosaurid temnospondyls (e.g., Ruta and Coates, 2007; Anderson, 2008; Sigurdsen and Green, 2011), seymouriamorphs would be stem amniotes (**Figure 1**). However, if crown amphibians would be considered more closely related to lepospondyls than any other clade, then seymouriamorphs would be stem tetrapods (e.g., Vallin and Laurin, 2004; Marjanović and Laurin, 2013). Recently, the monophyly of lepospondyls has been disputed (Pardo et al., 2017a). The monophyly of extant amphibians relative to amniotes is undisputed (San Mauro, 2010), but hypotheses of a polyphyletic origin with respect to Carboniferous and Permian 'early tetrapods' have been proposed several times by paleontologists, rooting salamanders, frogs and caecilians in different fossil groups (Anderson, 2007; Pardo et al., 2017a). In these frameworks, seymouriamorphs remain more closely related to amniotes than amphibians.

Even though we acknowledge the current debate on the origin of extant amphibians, we will consider here the most commonly accepted configuration in which batrachians originate within temnospondyls (Milner, 1988; Trueb and Cloutier, 1991; Schoch and Milner, 2004; Ruta and Coates, 2007; Anderson, 2008; Sigurdsen and Green, 2011; Pardo et al., 2017a; Schoch, 2018). As the affinities of caecilians are too uncertain, we will not indicate any marked preference for any hypothesis on their phylogenetic position. The phylogenetic framework we considered is summarized in **Figure 1** where seymouriamorphs will be regarded as stem amniotes (Anderson, 2007; Ruta and Coates, 2007; Klembara et al., 2014). We will nevertheless also discuss our results in the framework of the phylogenetic hypothesis proposed by Vallin and Laurin (2004) and Marjanović and Laurin (2013).

Material – Bones

Long-bone histology has been used and developed over decades to characterize the skeletal growth of tetrapods (Francillon-Vieillot et al., 1990; Sanchez et al., 2012). In the current study, we decided to study the humeri of two individuals of *S. sanjuanensis* (**Figures 2**, **3**) (Vaughn, 1966; Berman et al., 1987; Berman, 1993; Klembara et al., 2001) and one individual of *D. austriacus* (**Figure 4**) (Klembara, 1995; Klembara et al., 2001) (**Table 1**). The specimens MNG 7747 and CM 28597 were discovered associated with cranial and post-cranial skeletal elements in Lower Permian deposits (MNG 7747 – Berman et al., 1987; Berman, 1993; Klembara et al., 2001; CM 28597 – Vaughn, 1966; Berman et al., 1987). MNG 7747 is a small left humerus with an incipient supinator process (**Figure 2**; 17.21 mm long) assigned to a subadult individual based on the likeness and close size of its limb to that of a well-identified subadult specimen (ossified quadrate, no lateral line canals indicating that the specimen has already metamorphosed; Klembara et al., 2001, 2006). CM 28597 has been identified as the right humerus (**Figure 3**; 39.60 mm long) of an articulated large specimen whose skull length is almost twice larger than MNG 7747 (skull length of CM 28597 = 88 mm; Berman et al., 1987; skull length of MNG 7747 = 56 mm; Berman et al., 2000). The humerus of CM 28597 has a very well-developed supinator process. CM 28597 is as large as specimens identified as adults from the Tambach Formation (Berman et al., 2000). As for these fully mature specimens, the skull roof of CM 28597 exhibits a highly developed ornamentation with tightly closed sutures (Berman et al., 2000) and a well ossified braincase. SNM Z 15568 is one of the largest humeri of *Discosauriscus* known to date, measuring around 18.30 mm long (**Figure 4**), and it has been identified as the right humerus of a subadult specimen (Klembara and Bartík, 1999; Klembara et al., 2001; Sanchez et al., 2008; Klembara, 2009).

In order to discuss our results in a large evolutionary context, the stylopod of *S. sanjuanensis* and *D. austriacus* will be compared with those of Devonian tetrapods as well as temnospondyls. Because we had little data on the zeugopod bones of these comparative taxa, we deliberately decided to restrict our comparison to stylopods.

Method – Propagation Phase-Contrast Synchrotron Micro-Computed Tomography

The humeral microstructure of every specimen has been analyzed using PPC-SRμCT (Tafforeau et al., 2006) and three-dimensional

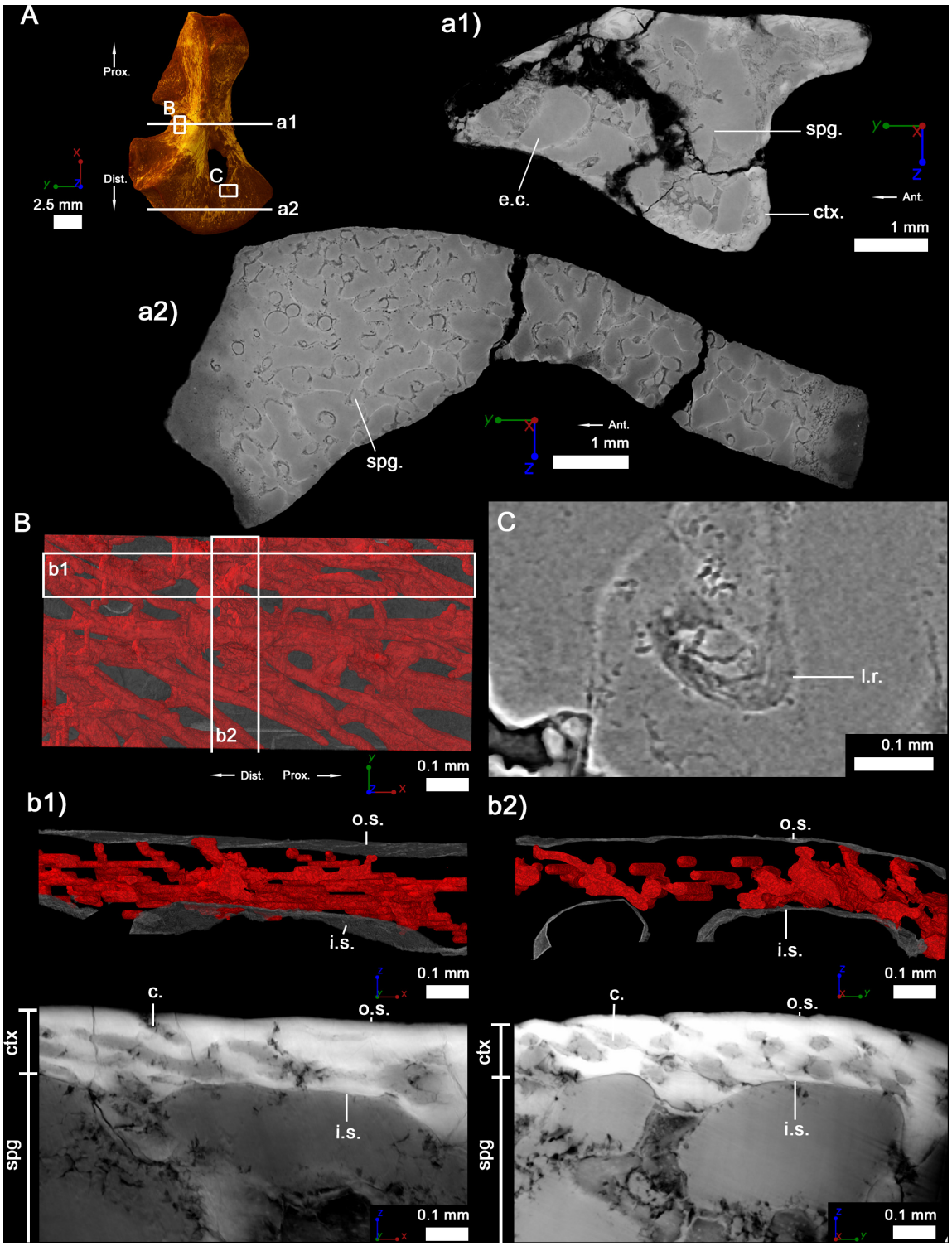

FIGURE 2 | Left humerus of a juvenile (subadult) specimen of *Seymouria sanjuanensis* (MNG 7747). **(A)** 3D model and virtual thin sections at midshaft **(a1)** and in the distal metaphysis **(a2)**. The arrows point toward the proximal (Prox.), distal (Dist.) and anterior (Ant.) directions. Both virtual thin sections **(a1,a2)** are 40 μm thick. **(B)** 3D model of the vascularization within the cortical bone at midshaft. The bony tissue is rendered in transparent gray and the cortical vascularization in red. A longitudinal **(b1)** and transverse **(b2)** 3D sections (100 μm thick and 1 mm long) were made in the cortical 3D model in **(B)**. Corresponding (20-μm-thick) virtual thin sections are presented under each 3D section. **(C)** Virtual thin section (thickness: 30 μm) showing the presence of Liesegang's rings. For each image, the red line of the tripod corresponds to the longitudinal axis, the green and blue to the transverse axes. c, vascular canal; ctx., cortex; e.c., empty cavity; i.s., inner surface of the cortical bone; l.r., Liesegang's ring; o.s., outer surface of the cortical bone; spg, spongiosa.

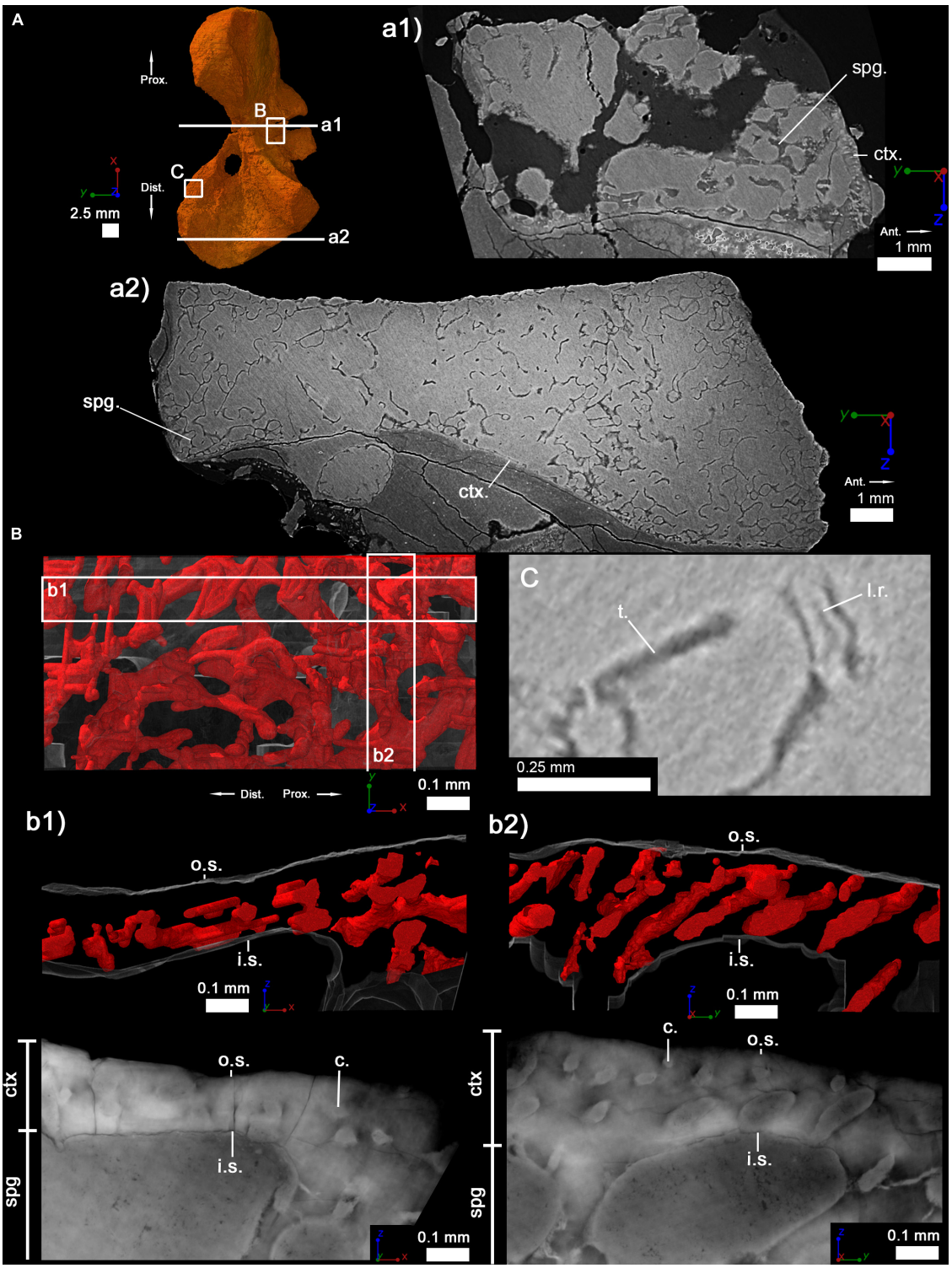

FIGURE 3 | Right humerus of an adult specimen of *Seymouria sanjuanensis* (CM 28597). **(A)** 3D model and virtual thin sections at midshaft **(a1)** and in the distal metaphysis **(a2)**. The arrows point toward the proximal (Prox.), distal (Dist.), and anterior (Ant.) directions. Both virtual thin sections **(a1,a2)** are 40 μm thick. **(B)** 3D model of the vascularization within the cortical bone at midshaft. The bony tissue is rendered in transparent gray and the cortical vascularization in red. A longitudinal **(b1)** and transverse **(b2)** 3D sections (100 μm thick and 1 mm long) were made in the cortical 3D model in **(B)**. Corresponding (20-μm-thick) virtual thin sections are presented under each 3D section. **(C)** Virtual thin section (60 μm thick) showing the presence of Liesegang's rings. For each image, the red line of the tripod corresponds to the longitudinal axis, the green and blue to the transverse axes. c, vascular canal; ctx., cortex; e.c., empty cavity; i.s., inner surface of the cortical bone; l.r., Liesegang's ring; o.s., outer surface of the cortical bone; spg, spongiosa; t., trabecula.

TABLE 1 | Information on the specimens studied.

Species	Ontogenetic stage	Bone	Bone length	Collection number	Collections	Formation	Geological age
Seymouria sanjuanensis	Subadult	Left humerus	17.21 mm	MNG 7747	Carnegie Museum of Natural History (Pittsburgh, United States)	Tambach Formation, Central Germany	Lower Permian
Seymouria sanjuanensis	Adult	Right humerus	39.60 mm	CM 28597	Museum der Natur (Gotha, Germany)	Cutler Formation, North-Central New Mexico, United States	Lower Permian
Discosauriscus austriacus	Subadult	Right humerus	18.30 mm	SNM Z 15568 (formerly K 52)	Slovak National Museum in Bratislava (Bratislava, Slovakia)	Letovice Formation, Boskovice Basin, Czechia	Lower Permian

(3D) virtual paleohistology (Sanchez et al., 2012). The specimens were imaged at the beamlines ID19 and BM05 of the European Synchrotron Radiation Facility (ESRF, France). A multiscale approach, consisting in a series of increasingly higher resolution scans, was used to study the samples of *S. sanjuanensis* (Tafforeau et al., 2007; Sanchez et al., 2012) from medium voxel sizes (14.96 and 6.96 μm respectively) to a submicron voxel size (0.75 μm) in regions of interest. The medium-resolution datasets reflect the entire bones imaged either in connection to the rest of the skeleton (CM 28597) or in isolated conditions (MNG 7747). The high-resolution scans were made in selected regions of the midshaft to infer aspects of the evolution and development of *S. sanjuanensis*' limbs down to the microscopic level. The humerus of *D. austriacus* was small enough to be imaged entirely with a voxel size of 3.03 μm which could reveal both the overall morphology and the microstructures of the bone relevant for the present study.

Technical Parameters for the Acquisition of the Scan Data of *S. sanjuanensis*

The medium-resolution scans were done on the ID19 beamline with a polychromatic beam, using a FReLoN 2k14 CCD detector (i.e., Fast Readout Low Noise CCD camera; Labiche et al., 2007) mounted on a Rodenstock optical system. For the lowest-resolution scans, the optics was associated to a 10 μm-thick Gadox (i.e., a Gadolinium oxysulfide powder) scintillator. The voxel size was therefore of 7.48 μm and ended up to 14.96 μm voxel size once the images were binned with a factor of 2. The distance between sample and detector was 960 mm. The experiment was performed with a W150 wiggler (11 dipoles, 150 mm of period) at a gap of 53 mm. The beam was filtered with 2 mm of aluminum and 6 mm of copper, thereby producing an average energy at the sample level of ∼106 keV. Considering the properties of the scintillator, the average detected energy (the effective energy that leads to the measured linear attenuation coefficients on the reconstructed slices) was ∼99 keV. The sample was imaged in half-acquisition, i.e., with the center of rotation shifted to the side of the field of view. 5000 projections were therefore necessary over 360° to reconstruct the final images. The exposure time per frame was of 0.3 s.

The 3.48 μm voxel size scans were performed on the ID19 beamline with the same FReLoN 2k14 CCD camera, coupled to an optical system associated to a 47 μm-thick $GGG:_{Eu}$ (i.e., a Gadolinium Gallium Garnet crystal doped with Europium) scintillator. The images were binned with a factor of 2, resulting in a final voxel size of 6.96 μm. The propagation distance was set to 700 mm. The beam spectrum was obtained by using the W150 wiggler at a gap of 37 mm, filtered with 2 mm of aluminum and 0.25 mm of tungsten. It resulted into an average energy of ∼83 keV, and a detected effective energy of ∼70 keV. In half-acquisition conditions, 4998 projections were recorded over 360° with an exposure time per frame of 0.15 s.

High-resolution scans (0.75 μm voxel size) were made using a $LuAG:_{Ce}$ scintillator of 25 μm thickness at mid-shaft. Because of the significant size difference between the isolated small humerus and the large humerus (still in connection to the rest of the skeleton within the sediment), different set-ups were used.

The mid-shaft of the small humerus (MNG 7747) was imaged at a propagation distance of 150 mm, using the W150 wiggler at a gap of 30 mm filtered with 0.05 mm of tungsten and 1 mm of aluminum. It resulted in a polychromatic beam with an average energy of ∼69 keV, and a detected effective energy of ∼62 keV. The optical microscope system adapted to white beam (long working distance mitutoyo 10x objective coupled with a 2x Olympus eyepiece) was associated to the FReLoN 2k14 CCD. 6000 projections over 360°, with an exposure time of 0.5 s per frame, were necessary to cover the field of view in half acquisition.

The mid-shaft of the large specimen (CM 28597) was imaged with a higher energy: 70 keV, using a beam monochromatized with a single 2.5 nm period W/B4C multilayer. The incoming beam was filtered with 2 mm of aluminum and 0.25 mm of copper to avoid total reflection of low energies on the multilayer substrate. The data was produced using a FreLON E2V CCD detector and a 6.2 μm GGG scintillator mounted on a microscope optic from Optic Peter using an Olympus 10 × 0.3 N.A. objective and a 2x Olympus eyepiece. The gaps of the U32u and U32d undulators were both set at 11.5 mm. In half-acquisition, 5000 projections were done over 360°, with a time of exposure of 1.6 s. The propagation distance between sample and detector was 200 mm. A 4 mm-thick spinning graphite disk, playing the role of a decoheror, was placed in the trajectory of the beam as close as possible of the multilayer to reduce the strong artifacts due to the defects of the multilayer.

Technical Parameters for the Acquisition of the Scan Data of *D. austriacus*

The experiment was conducted with a voxel size of 3.03 μm at beamline BM5 (bending magnet) of the ESRF. A 100 μm

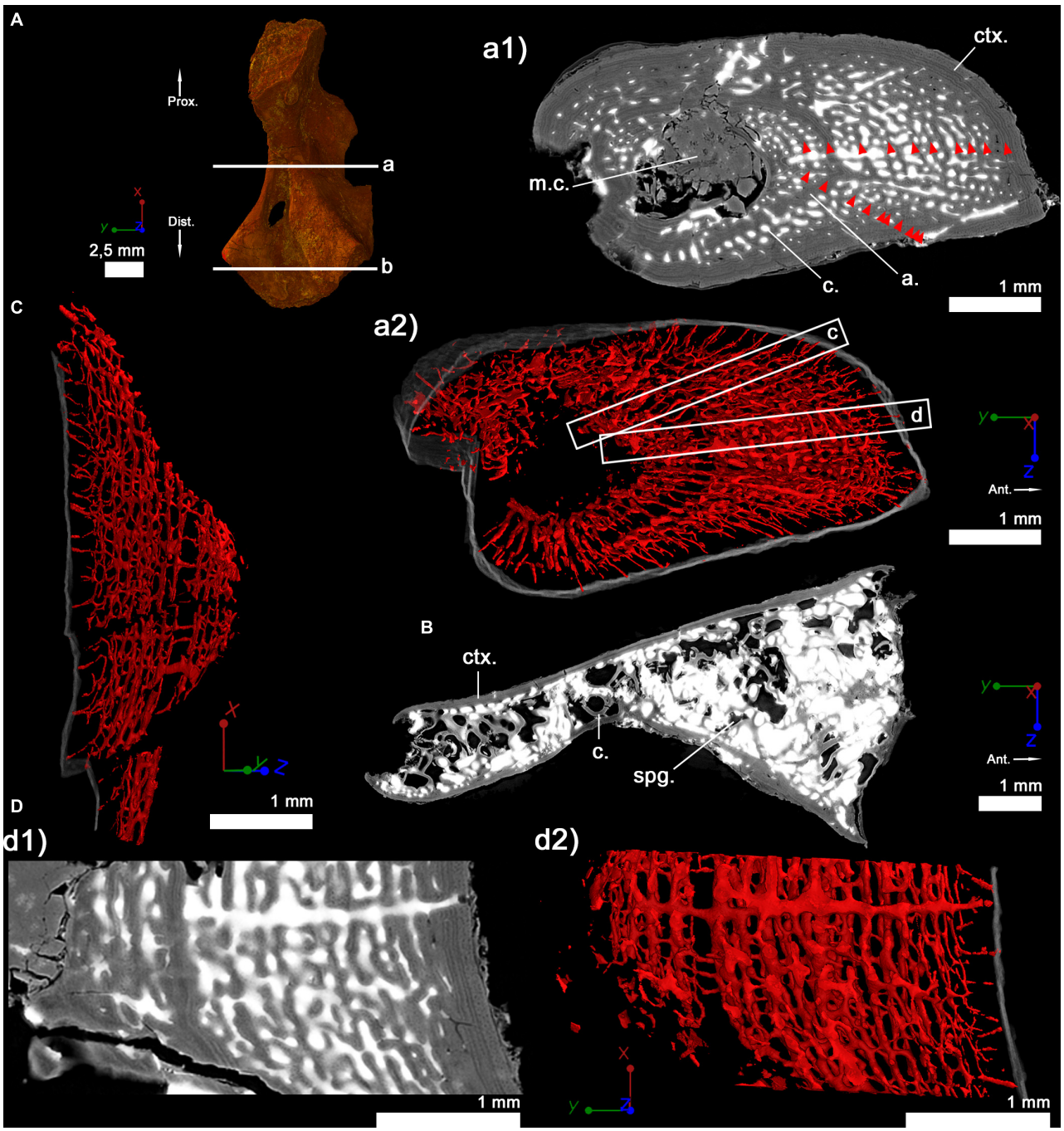

FIGURE 4 | Right humerus of a subadult specimen of *Discosauriscus austriacus* (SNM Z 15568). **(A)** 3D model and virtual thin sections at midshaft **(a)** and in the distal metaphysis **(b)**. The arrows point toward the proximal (Prox.) and distal (Dist.) directions. Both transverse virtual thin sections of the cortical bone at midshaft **(a1)** and in the metaphysis **(b)** are 40 μm thick. **(a2)** 600-μm-thick 3D section at midshaft. Red arrows in the midshaft transverse section **(a1)** point out lines of arrested growth. The bony tissue is rendered in transparent gray and the cortical vascularization in red. **(c)** Longitudinal 3D section of the shaft (thickness: 300 μm). **(D)** Longitudinal 40 μm-thick virtual thin section at midshaft **(d1)** and its corresponding 300-μm-thick 3D reconstruction **(d2)**. For each image, the red line of the tripod corresponds to the longitudinal axis, the green and blue to the transverse axes. a, annuli; c, vascular canal; ctx., cortex; m.c., medullary cavity; spg, spongiosa.

GGG:$_{Eu}$ scintillator was coupled with a 2.1x magnification optic (two Hasselblad photographic objectives mounted in tandem, HC 100 mm f/2.2 on the scintillator side – HC 210 mm f/4 on the sensor side) and a PCO Edge 4.2 sCMOS camera. The scan was made in half acquisition mode. The sample was place at 1360 mm from the detector and imaged using the 0.85 T bending magnet white beam filtered with 11 mm of aluminum, 6 mm of copper and 0.25 mm of molybdenum. The resulting

average energy was ∼120 keV, and the detected effective energy ∼112 keV. 6000 projections were taken over 360°. The exposure time was 0.1 s per frame.

Method – Image Reconstruction and Three-Dimensional Segmentation

Tomographic reconstruction was performed using the filtered back-projection algorithm implemented in the PyHST2 software (Mirone et al., 2014), integrating a single distance phase retrieval modified from Paganin et al. (2002) to integrate an unsharp mask of the retrieved phase maps before the tomographic reconstruction to compensate blurring effects (Sanchez et al., 2012). The reconstructed volumes were later filtered with a 3D unsharp mask to highlight more specifically the trabecular mesh.

Method – Virtual Bone Histology

This technique, although recently developed, has been thoroughly compared to classical bone histology based on physical thin sections (Sanchez et al., 2012). Apart from the collagen matrix organization, all the other bone microstructures (vascularization, cell lacunae, cementing lines of erosion, secondary deposits, lines of arrested growth, calcified cartilage remnants and Liesegang's rings) can be visualized as in real thin sections (Sanchez et al., 2012). In addition, 3D information can be extracted from virtual bone histology.

Virtual thin sections and 3D models were made using *VGStudio MAX* (versions 2 and 3, Volume Graphics, Inc., Germany) in the diaphyseal regions of the fossil long bones studied here. The midshaft is the region where bone development originates. It records the largest set of information regarding life-history traits (Francillon-Vieillot et al., 1990). Virtual thin sections were also made in the metaphyseal region to document the ossification process forming the spongiosa.

Method – Measurement Protocols

Cross-section, cortical and trabecular surfaces were measured for comparative purposes (**Tables 2**, **3**). The measurements were made using *VGStudio MAX* (version 3, Volume Graphics, Inc., Germany). Because the diaphysis of the studied humeri is not circular, the thickness of the cortical bone (when present) was measured in 10 different locations (**Table 2** and **Figures 5A1,B1,C1,C3**). Lines of arrested growth were identified in the specimen SNM Z 15568 of *D. austriacus* (**Figure 4a1**). Due to the extension of the cortical bone under the humeral crest, the distance between two LAGs was measured at two different locations to obtain an average distance for each growth mark (**Figure 4a1** and **Table 4**). The diameters of the cortical vascular canals (**Table 2**) and maximal length of the cell lacunae (**Figure 6**) were averaged from 10 measurements distributed equally along the areas analyzed. Because the periphery of the compact cortical bone was obscured by a metallic infilling during the fossilization in both specimens of *S. sanjuanensis*, the vascular canals and cell spaces were measured at a few hundreds of micrometers from the surface of the cortex (**Figures 2**, **3**, **6**). As the cortical bone deposit of *D. austriacus* displays an obvious cyclical pattern with LAGs, the diameter of the cortical canals was measured in 10 annuli and 10 zones of several growth marks (Francillon-Vieillot et al., 1990), all distributed equally between the inner region of the cortex, the middle core of the cortex and the outer part of the specimen (**Table 2**). The trabecular thickness was also calculated as the average of 10 measurements in sections made at midshaft and in the metaphysis – except in the cases for which less than 10 trabeculae were present (e.g., midshaft of *D. austriacus* which comprises only 2 trabeculae; **Figures 5**, **7** and **Table 2**).

Virtual thin sections were converted into binary images with *Photoshop CS6* (version 13.0, x64, Adobe, Inc., United States) and constituted the bases for measuring the trabecular area of each section. The *trabecular area* is defined as the ratio between the area occupied by the spongiosa over the total area covered by the cross-section area (**Figures 5A2,B2,C2,C4**). It is given here in percentage (**Table 3**). In the case of damages on the cortex due to fossilization (e.g., cracks, unpreserved regions), we decided to restore the missing cortical parts (only if they were restricted to localized areas) by extending the bone surface while maintaining a constant thickness of the cortical bone (**Figure 5**). Bone compactness was also measured from these binary thin sections for each sample (**Figures 5A2,B2,C2**). Compactness profiles are provided in **Figure 8**. They were produced using the software *Bone Profiler* (Girondot and Laurin, 2003).

RESULTS

Mid-Diaphyseal and Metaphyseal Bone Histology of the Humerus of the Juvenile (Subadult) *Seymouria sanjuanensis* (MNG 7747)

Transverse sections, made in the metaphyseal and diaphyseal regions (**Figures 2Aa1,a2**), reveal a very spongy microanatomy (confirmed by the longitudinal sections made in **Figure 7**).

In the diaphysis, the cortex forms a thin layer (189 μm) of compact bone, which becomes thinner toward the ossification notch (**Table 2**). The spongiosa is built up by numerous trabeculae (**Table 3**), 94 μm thick, which are unevenly distributed in the medullary cavity. The trabecular area covers around 74% of the total bone area in cross section (**Table 3**). This trabecular arrangement results in the formation of a large empty cavity in the anterior region of the midshaft and in several smaller interconnected cavities surrounding this main central cavity (**Figures 2a1**, **7**). There is a clear separation between the loose spongiosa and the compact cortical bone (**Figures 2a1,a2**) as supported by the compactness profile (**Figure 8A**). No lines of arrested growth (LAG) nor annuli were found anywhere in the cortical bone (**Figures 2b1,b2**). The pattern of vascularization at midshaft is characterized by a dense mesh of large canals (**Figure 2B**). The canals (which are 40 μm of diameter on average, **Table 2**), appear obliquely oriented (with an overall longitudinal orientation) in most of the cortex (**Figures 2b1,b2**). Some of them present some anastomoses. They slightly curve radially just under the surface of the bone to cross the outer surface with a less acute angle (**Figures 2b1,b2**).

TABLE 2 | Raw data measurements (cross-section diameter, cortical thickness, trabecular thickness, and canal diameter) from the humeri of *Seymouria sanjuanensis* and *Discosauriscus austriacus* following the protocol we present in Section "Materials and Methods."

Specimen	**Diaphysis**				**Metaphysis**	
Subadult *Seymouria sanjuanensis* (MNG 7747)	**Figure 2a1**			**Figure 2B**	**Figure 2a2**	
	Cross-section diameter	**Cortical thickness**	**Trabecular thickness**	**Canal diameter**	**Cortical thickness**	**Trabecular thickness**
	5640	430	100	40	NA	40
	3600	100	70	40		20
	2830	110	130	40		20
	3300	220	40	40		20
		170	130	50		30
		90	70	50		40
		220	50	30		20
		250	60	50		20
		200	180	30		20
		100	110	30		20
Adult *Seymouria sanjuanensis* (CM 28597)	**Figure 3a1**			**Figure 3B**	**Figure 3a2**	
	Bone width	**Cortical thickness**	**Trabecular thickness**	**Canal width**	**Cortical thickness**	**Trabecular thickness**
	8390	270	70	50	NA	30
	7130	270	50	50		30
	3880	500	60	70		30
		210	100	20		30
		150	90	30		30
		100	70	50		40
		200	110	90		40
		310	40	30		30
		90	80	30		20
		120	120	40		20
Subadult *Discosauriscus austriacus* (SNM Z 15568)	**Figure 4a1**			**Figure 5C5**		**Figure 4b**	
	Bone width	**Cortical thickness**	**Trabecular thickness**	**Canal width**			**Cortical thickness**	**Trabecular thickness**
				Inner (I)	**Middle (M)**	**Outer (O)**		
	5760	750	80	20	50	20	210	50
	5370	850	90	70	40	30	150	60
	2670	1240	70	30	30	20	150	60
	2600	630	80	40	60	20	220	70
		3140		20	50	20	170	30
		2780		20	50	20	140	60
		810		20	30	20	310	40
		860		30	30	20	150	70
		1260		10	40	10	130	50
		2060		50	50	20	160	50

As many measurements as possible – up to 10 – were taken and averaged to provide representative data which we present in Section "Results."

Osteocyte lacunae are numerous in the outermost compact cortex (**Figure 6A**). The maximal length of the bone cell lacunae is 10.3 μm long on average. Most of the cell lacunae are rounded or triangular and a few are slightly flattened (**Figure 6A**). There is no sign of endosteal ossification along the shaft (**Figures 2b1,b2**).

In the metaphyseal region, the cortex is mostly non-existent or very reduced (**Figure 2a2**). The spongiosa is homogeneously distributed and relatively dense. It is formed of very thin trabeculae (25 μm, **Table 3**). A few scattered remnants or Liesegang's rings of calcified cartilage can be observed (**Figure 2C**).

TABLE 3 | Microanatomical measurements in the subadult humerus of *Seymouria sanjuanensis* (MNG 7747), the adult humerus of *Seymouria sanjuanensis* (CM 28597), and the subadult humerus of *Discosauriscus austriacus* (SNM Z 15568).

Cross sections	Diaphysis (a1)	Metaphysis (a2/b)
***Seymouria sanjuanenis* MNG 7747**		
Trabecular area	73,64%	100%
Cortical bone thickness	189 μm	0 mm
Trabecular thickness	94 μm	25 μm
***Seymouria sanjuanenis* CM 28597**		
Trabecular area	85,60%	100%
Cortical bone thickness	222 μm	0 mm
Trabecular thickness	79 μm	30 μm
***Discosauriscus austriacus* SNM Z 15568**		
Trabecular area	41,68%	87,56%
Cortical bone thickness	857–2310 μm	179 μm
Trabecular thickness	80 μm	54 μm

*Measurements are made on the cross-sections at midshaft and in the metaphyses (illustrated in **Figures 2–4**) using the protocol detailed in Section "Materials and Methods."*

Mid-Diaphyseal and Metaphyseal Bone Histology of the Humerus of the Adult *Seymouria sanjuanensis* (CM 28597)

In the locations where it is preserved, the compact cortical bone in the diaphysis is almost as thin as in the juvenile described above (222 μm) (**Figure 3a1** and **Table 3**). The trabecular area covers about 86% of the total surface of the transverse bone section (**Table 3**) in the shaft. The metaphyseal cortical bone is almost non-existent in the adult (as in the juvenile) (**Figure 3a2**). The thickness of the trabeculae in the spongiosa measures 79 μm in the diaphysis at the adult stage and 30 μm in the metaphysis (**Table 3**).

Although heavily fractured, the microstructure of the diaphysis is relatively well-preserved in three dimensions (**Figure 3a1**). The trabeculae are distributed homogeneously in the anterior region but an empty space is obvious in the posterior part of the medullary cavity (**Figures 3a1**, **7B**). The compactness profile clearly reveals the extension of the spongiosa and the decrease of the thickness of the compact cortex (**Figure 8B**). Once again, the compacta and spongiosa are clearly distinguished (**Figures 3a1,a2**). As in the smaller specimen, the cortical bone of CM 28597 does not present any evidence of LAGs nor annuli (**Figures 3b1,b2**). The vascularization of the cortex is composed of a layer of radially-oblique canals (**Figures 3b1,b2**). The overall orientation is not anymore longitudinal but more radial in the adult specimen (**Figure 3b2**). The vascular mesh seems somewhat more anastomosed and disorganized than in the juvenile. The mean diameter of the canals is 46 μm in the adult specimen (**Table 2**). The density of cell spaces has slightly decreased compared to the juvenile but remains relatively high in the outermost compact cortex (**Figure 6**). The mean maximal length of these osteocyte lacunae however has obviously reduced by half (5 μm, **Figure 6**). The cell lacunae are still rounded though.

The spongiosa in the metaphysis of the adult specimen (CM 28597) seems as dense as in the juvenile specimen (**Figure 3a2**). Due to remodeling events, it is not as homogeneous as in the juvenile (**Figure 2a2**). Remnant of calcified cartilage (Liesegang's rings) are barely visible (**Figure 3C**).

Mid-Diaphyseal and Metaphyseal Bone Histology of the Humerus of the Subadult *Discosauriscus austriacus* (SNM Z 15568)

The diaphyseal bone histology of a growth series of *D. austriacus* has already been described on the basis of 2D thin sections (Sanchez et al., 2008). Here we provide an additional and complementary description based on 3D observations. At midshaft, the cortical thickness varies between 857 μm (in the posterior region) and 2310 μm (under the process in the anterior region) (**Figure 4a1**). The trabecular area only occupies 42% of the cross section (**Table 3** and **Figure 5C2**). As demonstrated by the binary image (**Figure 8C**), the medullary cavity is not as spongy as in the adult *S. sanjuanensis*. It is small and crossed by two 80-μm-thick trabeculae in *D. austriacus* (**Figure 4a1** and **Tables 2**, **3**). The cortex shows annuli and LAGs in both the diaphysis and metaphysis (**Figures 4a1**, **9**). A 3D transverse section reveals that the cortical vascularization is essentially made of oblique canals radiating from the innermost to the outermost layer of the cortex (**Figure 4a2**). Longitudinal sections show that there is as well a very strong longitudinal component of the vascular mesh showing an overall crisscrossed network of vascular canals (**Figure 4c**). In transverse view, the longitudinal canals are organized in a circular pattern (**Figure 4a2**). The vascular pattern is cyclically interrupted by annuli and LAGs (**Figures 4a1**, **9**). Ten LAGs could be identified in this humerus (**Figure 4a1**) as in the tibia of the same individual of *D. austriacus* SNM Z 15568 studied by Sanchez et al. (2008). The mean distance between two LAGs in the humerus is 202 μm (**Figure 4Aa1**). The mean diameter of the cortical vascular canals at midshaft ranges from 20 μm in the annuli (i.e., cyclical thin bone deposits corresponding to periods of slow growth rate, Francillon-Vieillot et al., 1990) to 70 μm in the zones (i.e., cyclical thick bone deposits corresponding to periods of high growth rate, Francillon-Vieillot et al., 1990). The cell lacunae in the periosteal bone are as large as in the juvenile specimen of *S. sanjuanensis* (10.2 μm on average; **Figure 6C**) and their density is relatively high (especially in the zones, **Figure 6**). The cell lacunae are rounded. This confirms the data observed on other limb bones by Sanchez et al. (2008).

The cortex in the metaphysis is 179 μm thick (**Figure 4b**). The spongiosa occupies 88% of the entire area of the section (**Table 3** and **Figure 5C4**). The trabeculae in the metaphysis are 54 μm thick (**Table 3** andf **Figure 4b**) and are distributed homogeneously. A secondary bone deposit is visible on the surface of the trabeculae. No obvious remnants of calcified cartilage can be observed in the bone. This observation confirms

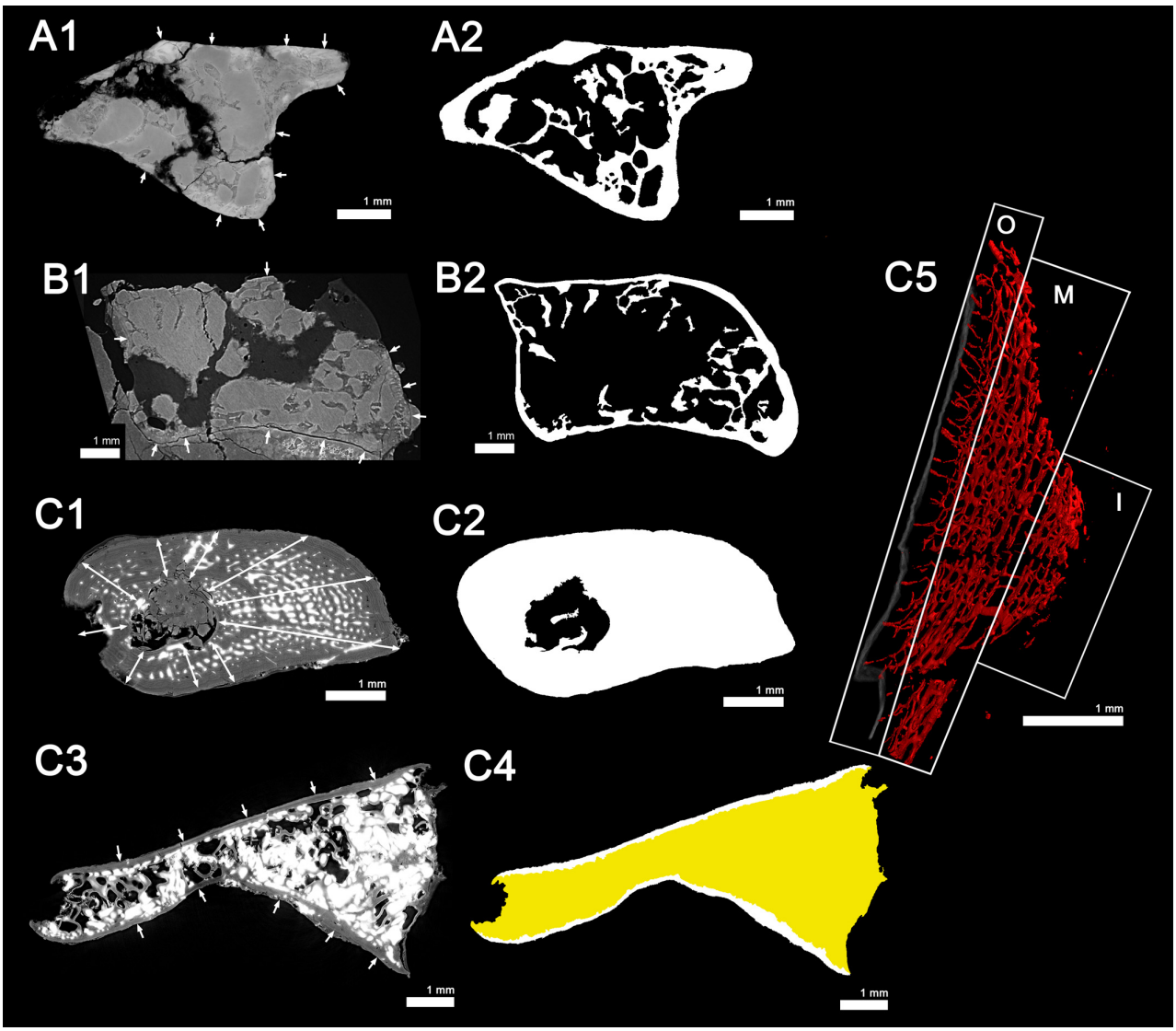

FIGURE 5 | Cross-section measurements: **(A1,A2)**, the juvenile (subadult) *Seymouria sanjuanensis* (MNG 7747); **(B1,B2)**, the adult *S. sanjuanensis* (CM 28597); and **(C1–C5)** the subadult *Discosauriscus austriacus* (SNM Z 15568). All virtual thin sections are 40 μm thick. **(A1,B1,C1)** show the locations (white arrows) where the cortex thickness was measured at midshaft. C3 shows the locations (white arrows) where the cortical thickness was measured in the metaphysis of *D. austriacus*. **(A2,B2,C2,C4)** illustrate the area occupied by the spongiosa and the total area covered by the cross-section area at midshaft **(A2,B2,C2)** and in the metaphysis (compacta in white and spongiosa in yellow) **(C4)** used for the calculation of the *trabecular area*. **(C5)** Shows the three areas where the cortical canals were measured (I, inner cortex; M, middle cortex; O, outer cortex; **Table 2**).

previous investigations in other specimens of *D. austriacus* (Sanchez et al., 2008).

DISCUSSION

Limb Bone Growth of Seymouriamorphs

Humeral Growth of *Seymouria sanjuanensis*

The compact vascularized deposit forming a cortical cylinder surrounding the humeri of the juvenile and adult specimens of *S. sanjuanensis* results from periosteal ossification as in (stem- and crown-) tetrapods (Francillon-Vieillot et al., 1990; Sanchez et al., 2008, 2010a, 2014, 2016). Remnants of Liesegang's rings within the metaphysis (**Figures 2C**, **3C**) are typical of tetrapod calcified cartilage resulting from endochondral ossification (Francillon-Vieillot et al., 1990). The parallel and longitudinal orientation of the trabeculae found in the humeral metaphyses of the juvenile and adult *S. sanjuanensis* (**Figure 7**) typically results from the development of a growth plate (Francillon-Vieillot et al., 1990; Sanchez et al., 2014) that permits the elongation of these bones. The humerus of *S. sanjuanensis* thus develops as in extant tetrapods, allowing us to use bone microstructure criteria from extant tetrapods (Francillon-Vieillot et al., 1990) to interpret its life-history traits.

TABLE 4 | Cyclical bone deposit values in the stylopod bones of *Discosauriscus austriacus*, *Acanthostega gunnari,* and *Doleserpeton annectens*.

	Discosauriscus **(femoral values from Sanchez et al., 2008)**	***Acanthostega*** **(from Sanchez et al., 2016)**	***Doleserpeton*** **(S.S. personal observation on the thin section 919.5.3T from the MNHN)**
Mean bone deposit between consecutive lines of arrested growth	Humerus: 202 μm Femur: 26–82 μm	Humerus: 65 μm	Femur: 36 μm

Measurement of the distance between two consecutive lines of arrested growth (LAGs) with a minimum of 6 measurements for each sample.

Although the adult specimen of *S. sanjuanensis* still exhibits a few remnants of calcified cartilage (**Figure 3C**), their occurrence is very scattered and their number has clearly decreased since the juvenile stage (**Figure 2C**), thereby suggesting that the trabecular mesh was significantly and actively remodeled during the development. The rearrangement of the spongiosa in the adult (**Figure 7**) supports this remodeling hypothesis.

The cortical bone is compact and deposited by appositional growth (**Figure 6**). The density of the cortical vascularization at midshaft in *S. sanjuanensis* remains unchanged through its ontogeny (**Figures 2B**, **3B**). The relative volume of the vascular mesh also remains identical between both developmental stages. The cell lacunar density stays relatively high from the juvenile to the adult stage and the cell lacunae remain rounded but their size reduces by half (**Figure 6**). The lack of endosteal bone in *S. sanjuanensis* (**Figure 6**) together with the intense erosion of the cortex, its dense vascularization and the large size of the vascular canals, as well as the high density of cell lacunae and their rounded shape, in both specimens are indicative features of active bone dynamics, even at the adult stage. The density of the vascularization seems to be correlated with the growth rate in most vertebrates (e.g., de Buffrénil et al., 2008; Padian, 2012; Cubo et al., 2014) except anurans (Canoville et al., 2018). No LAGs were found in the cortices of any of the studied specimens (**Figure 6**). Very few groups of tetrapods show no LAGs, even in endothermic animals (Bourdon et al., 2009; Köhler et al., 2012). Only some birds and dinosaurs do so: the absence of LAGs associated to fibrolamellar bone in dinosaurs, is linked to very fast growth (Sander et al., 2004; Padian, 2012); the absence of LAGs in extant birds is due to the fact that they almost all grow in a year (van Soest and van Utrecht, 1971; Padian et al., 2001) and their skeleton is lightened by internal erosion in response to flying constraints (Cubo and Casinos, 2000; de Margerie et al., 2005). **Figure 10** clearly shows that no cortical bone from the juvenile individual persists in the cross-section of the adult humerus as the result of intense erosion. The absence of LAGs in the humerus of *S. sanjuanensis* therefore probably results from fast bone deposition coupled to an intense erosion process giving rise to a thin incomplete cortical bone record. For this reason, no skeletochronological analysis could be performed.

Humeral Growth of *Discosauriscus austriacus*

The diaphyseal histology of *D. austriacus* was previously described on the basis of 2D transverse diaphyseal thin sections of various long bones (including humeri and femora) (Sanchez et al., 2008). A skeletochronological analysis was conducted. Based on the identification and measurement of growth rate between LAGs, Sanchez et al. (2008) could determine the developmental stage of each individual. They studied both stylopodial and zeugopodial bones. Most zeugopods were well-preserved due to their high compactness (**Figures 1a–d** in Sanchez et al., 2008). However, all stylopods were unfortunately largely broken during the fossilization process because of their spongy microanatomy (**Supplementary Figure 1B**). For this reason, assuming that the cortical thickness of these bones was equal along the diaphysis (as in most extant tetrapods), they sectioned the bones at different levels of the shaft. All stylopods studied in 2008 showed very thin cortices (**Supplementary Figure 1Ba** and **Figure 11B**). The current study exhibits a very thick diaphyseal cortex in an exceptionally 3D well-preserved humerus (SNM Z 15568, **Figures 4a1**, **11A** and **Supplementary Figure 1Ac**). In order to understand this difference between both sets of sections, a longitudinal virtual thin section was made in this humerus (SNM Z 15568, **Supplementary Figure 1Aa**). It reveals that the thickness of the humeral cortical bone very rapidly decreases from either side of the midshaft where the long-bone growth originates (**Supplementary Figure 1Ad**). This means that the complete periosteal record is restricted to about 300–500 μm of the diaphysis. The difference between the thin sections made in Sanchez et al. (2008) and our virtual transverse thin section is therefore probably due a different conception of the diaphysis geometry (**Supplementary Figure 2**). In the case of a hour-glass geometry of the shaft with a restricted complete periosteal record (as for the humerus of *D. austriacus*), the distance between LAGs drastically varies between the exact center of diaphyseal growth and way out of the diaphyseal growth center (**Supplementary Figure 2**). The virtual thin section made in the humerus of SNM Z 15568 also shows that the vascularization drastically decreases toward the metaphyses paralleling the tightening of the LAGs toward these regions of the bone (**Supplementary Figures 1Ab–d**). In 2008, it was therefore almost impossible to locate the exact center of growth without X-rays and do multiple sections in the short diaphysis of the humeri of *D. austriacus* (due to the 300-μm thickness of the saw and the poor preservation of the fossil material allocated to thin sectioning in 2008; **Supplementary Figure 1B**). All humeri sectioned by Sanchez et al. (2008) exhibited a very thin cortex with tight LAGs associated with a poor vascularization as the virtual section made proximally in the diaphysis of SNM Z 15568 (**Supplementary Figure 1Ab**). Similarly, Sanchez et al. (2008) showed a slightly vascularized primary bone in the outermost cortex of the femur of SNM Z 15568 (**Figure 11**) which fits with the outermost layer of the

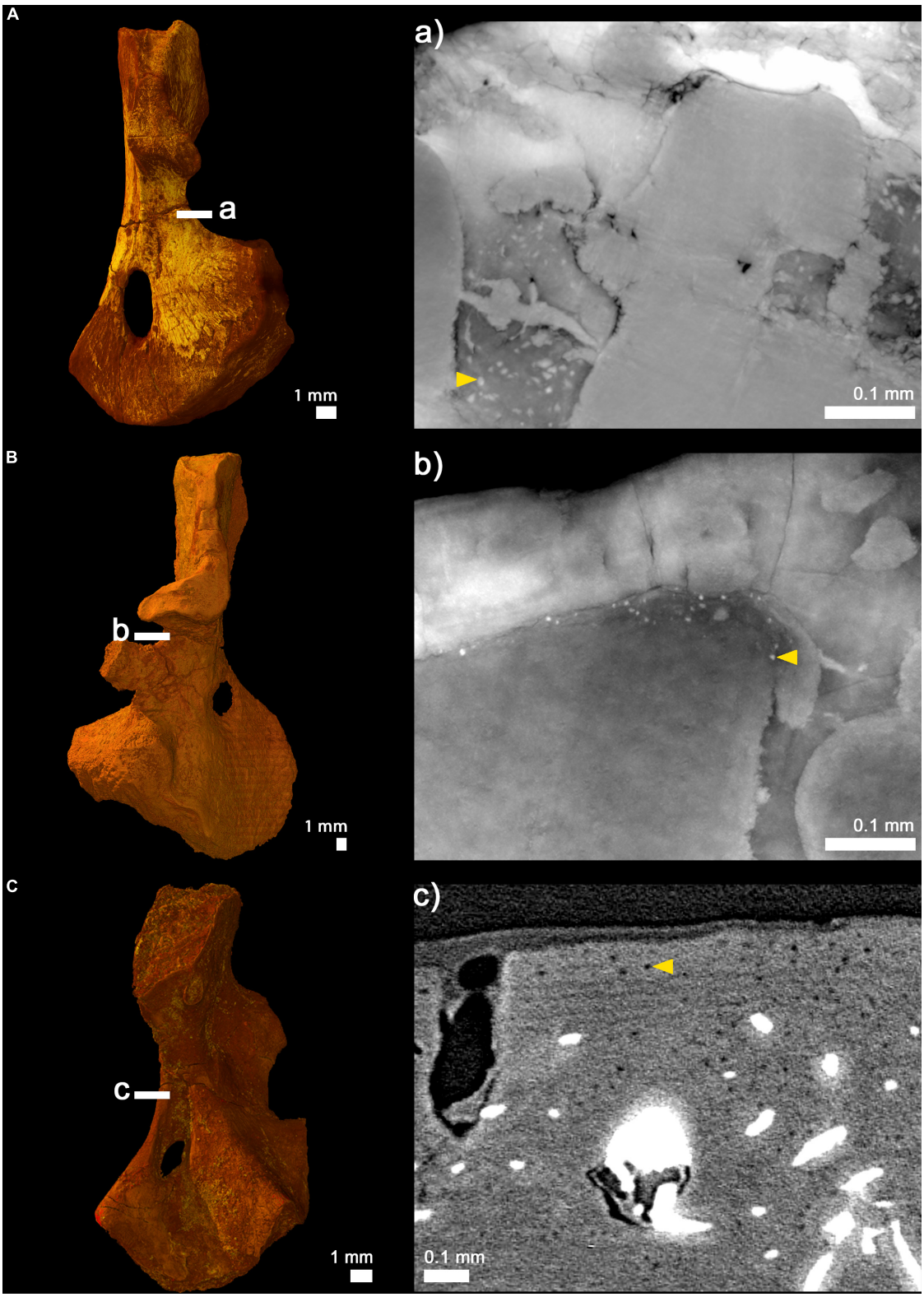

FIGURE 6 | Cortical virtual thin sections showing cell lacunae. **(A)** 3D model of the humerus of the juvenile (subadult) *Seymouria sanjuanensis* (MNG 7747) showing the location where the 20-μm-thick virtual thin section was made **(a)**. **(B)** 3D model of the humerus of the adult *S. sanjuanensis* (CM 28597) showing the location where the 20-μm-thick virtual thin section was made **(b)**. **(C)** 3D model of the humerus of the subadult *Discosauriscus austriacus* (SNM Z 15568) showing the location where an image was made **(c)**. Yellow arrows point out one example of cell lacunae for each section.

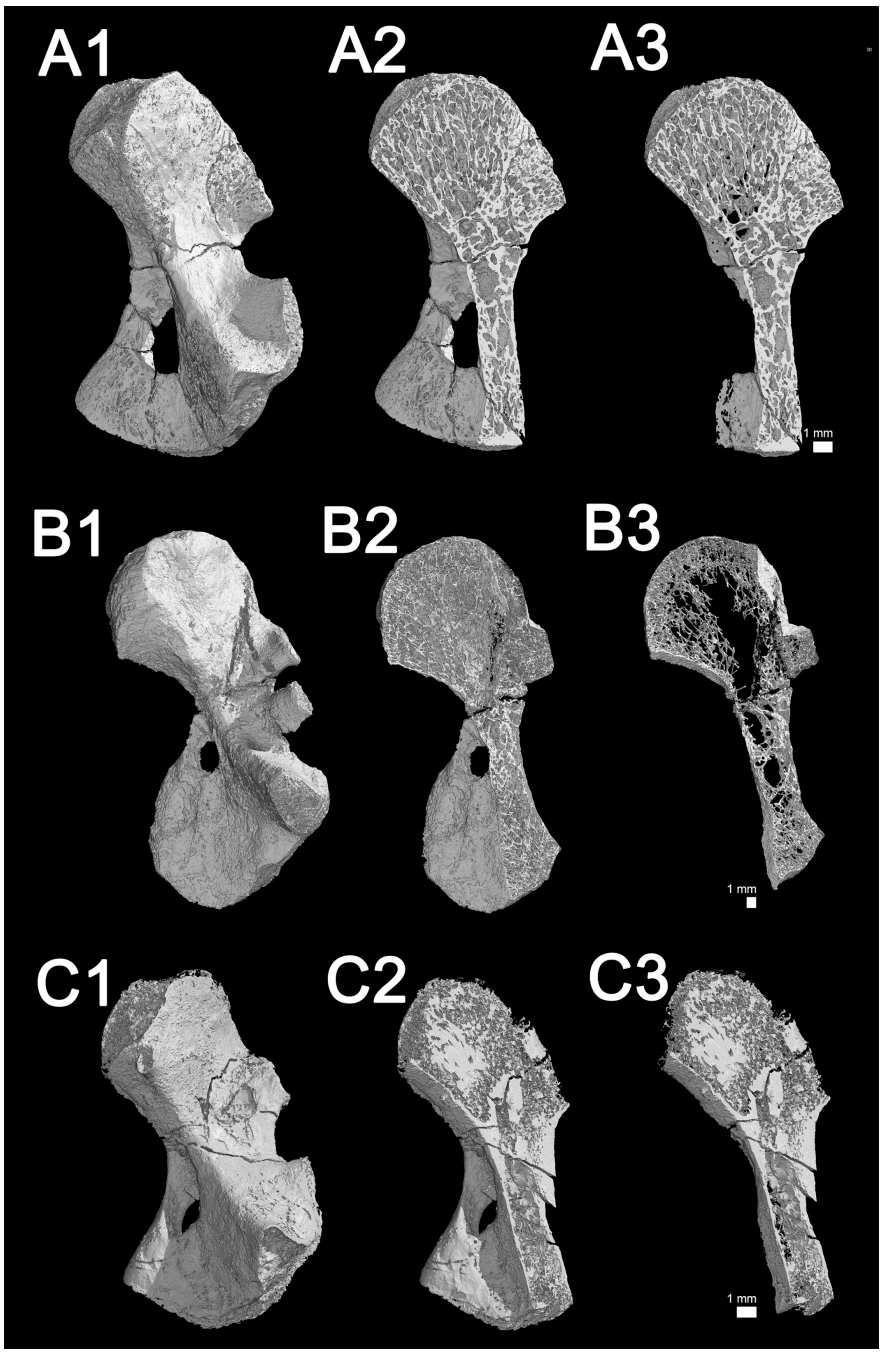

FIGURE 7 | Microanatomy 3D models of the juvenile (subadult) humerus of *Seymouria sanjuanensis* (MNG 7747, **A1–3**), the adult humerus of *S. sanjuanensis* (CM 28597, **B1–3**) and the subadult humerus of *Discosauriscus austriacus* (SNM Z 15568, **C1–3**). **(A1,B1,C1)** Complete 3D models. **(A2,B2,C2)** Sectioned models showing the spongiosa. **(A3,B3,C3)** 1 mm-thick sections through the spongiosa. The image of the humerus of MNG 7747 **(A1,A2,A3)** has been inverted afterward (as if it was a left humerus) for comparative purposes.

midshaft humeral cortex of the same individual (SNM Z 15568, **Supplementary Figure 1Ab**).

The vascularization in the innermost region of the 3D thin section (in the humerus of *D. austriacus*, SNM Z 15568) actually exhibits a dense network of oblique canals organized in rows and alternating with annuli (**Figures 4a1,a2**). This configuration resembles the dense vascular mesh observed in *S. sanjuanensis* (**Figures 2B**, **3B**) except that the erosion is not as intense in *D. austriacus* as it is in *S. sanjuanensis*. Sanchez et al. (2008) interpreted the poorly vascularized and sublamellar shaft histology of *D. austriacus* as the result of "a relatively slow, well-organized bone deposition." This was supported by a poorly

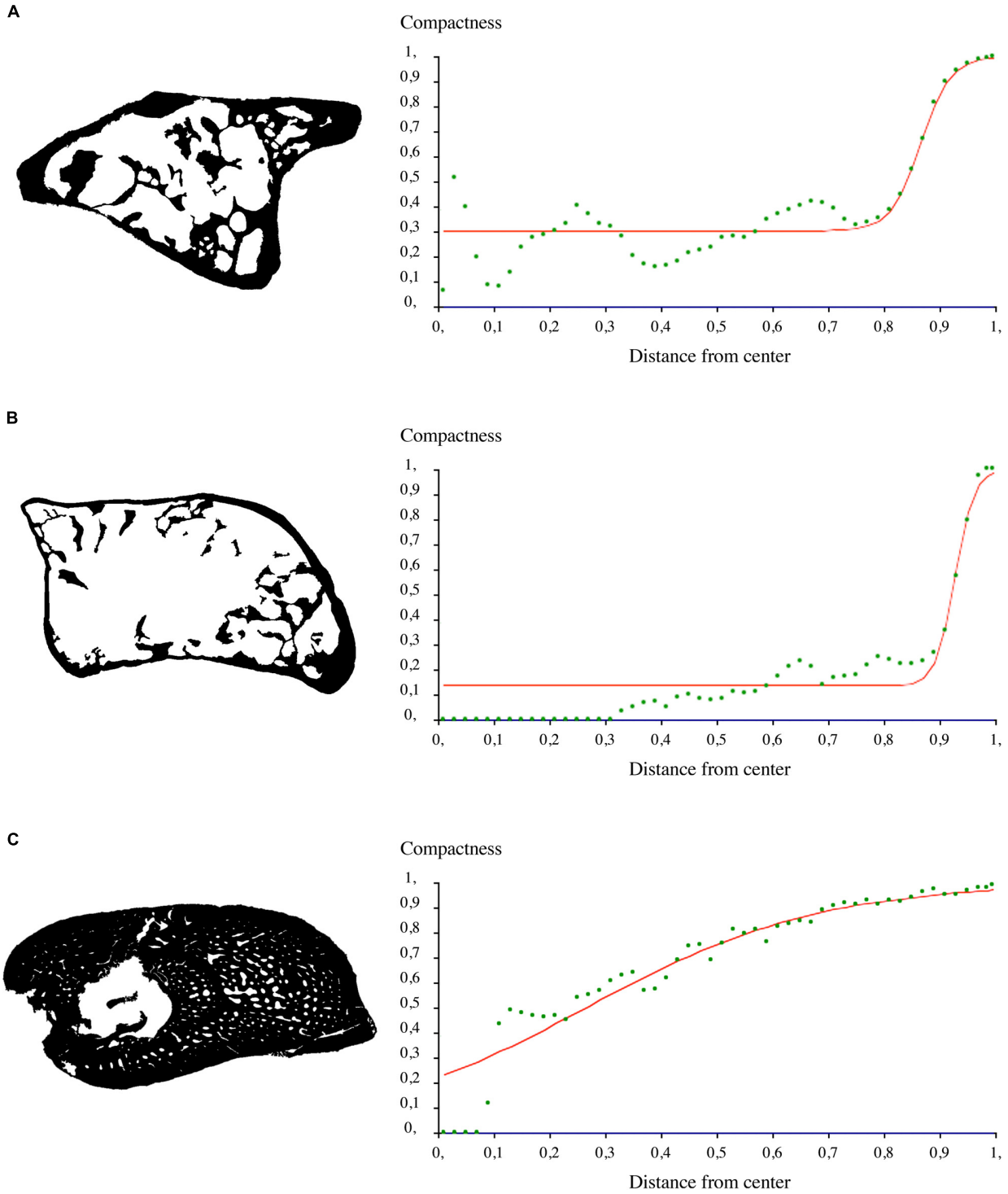

FIGURE 8 | Compactness profiles of midshaft sections. **(A)** Binary section made in the humerus of the juvenile (subadult) *Seymouria sanjuanensis* (MNG 7747) and the corresponding compactness profile. **(B)** Binary section made in the humerus of the adult *S. sanjuanensis* (CM 28597) and the corresponding compactness profile. **(C)** Binary section made in the humerus of the subadult *Discosauriscus austriacus* (SNM Z 15568) and the corresponding compactness profile.

vascularized (pseudo-)lamellar tissue. The denser vascularization of the inner core of the current 3D model of the humerus (**Figures 2B**, **3B**) would tend to contradict this former claim at least for the stylopod bones of *D. austriacus*. We would rather describe the midshaft bone of *D. austriacus*' stylopod as more active than previously thought. This is consistent with (1) the

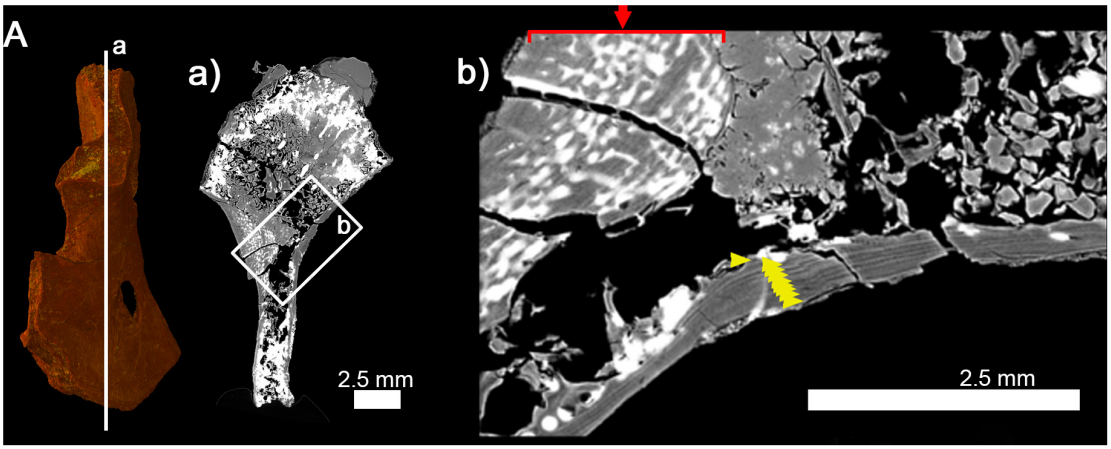

FIGURE 9 | Histology of the right humerus of *Discosauriscus austriacus* (SNM Z 15568). **(A)** 3D model. **(a)** Longitudinal thin section (thickness: 40 μm) showing a thick extremely-vascularized cortex and lines of arrested growth running along the entire shaft. **(b)** Detail of **(a)** showing the thick vascularized cortex (red arrow) and lines of arrested growth in the outermost part of the cortical bone (yellow arrows).

relatively great density of cell lacunae in the cortex and the rounded shape of these lacunae (**Figure 6**); (2) the absence of calcified cartilage in the entire humerus which suggests a relatively fast endochondral ossification (Sanchez et al., 2008). We observe a faster average annual growth rate in the humerus (202 μm/year, **Figure 4a1** and **Table 4**) than in the femur (26–82 μm/year, Sanchez et al., 2008). The numerous LAGs observed in the humerus of SNM Z 15568 show that the individuals of *D. austriacus* alternated short fast growing periods with lethargic periods probably to accommodate environmental conditions, presumably extreme lake fluctuations under a tropical climate (Klembara and Meszároš, 1992). This resulted in an overall relatively fast depositional dynamic.

Conclusion on Seymouriamorphs

These 3D observations on both *S. sanjuanensis* and *D. austriacus* suggest that seymouriamorphs had a faster humeral growth than previously suggested (Sanchez et al., 2008). These conclusions are preliminary as only based on comparative stylopodial data within two species. Zeugopods – exhibiting a thicker cortex in seymouriamorphs, than in temnospondyls and stem tetrapods (Sanchez et al., 2008, 2010a, 2014) – will need to be investigated to complete the current investigation. More seymouriamorphs should also be studied.

Evolution of Limb Bone Growth in Non-amniotic Tetrapods

Within seymouriamorphs, only the limb bone histology of *D. austriacus* and *S. sanjuanensis* has been investigated so far (including the current study). Would this limb bone histology differ or resemble that of earlier forms of tetrapods?

The humeral histology of the stem tetrapod *Acanthostega* (**Figure 1**) (whose length reaches about one meter maximum for the largest juvenile known so far) displays a primary bone often poorly vascularized (except in localized regions such as muscle attachments) and punctuated by LAGs (65 μm/year, **Table 4**; Sanchez et al., 2016). The innermost surface of the cortex is uneroded. This all suggests an extremely slow bone deposition and a slow development of the humerus which greatly contrasts with the humeral histology of seymouriamorphs.

Previous histological studies on the humerus of temnospondyls (**Figure 1**) have shown a great diversity of bone patterns with a large range of cortical vascular densities and growth rates (de Ricqlès, 1979, 1981; Steyer et al., 2004; Laurin et al., 2006; Witzmann, 2009; Mukherjee et al., 2010; Sanchez et al., 2010a,b; Konietzko-Meier and Klein, 2013; Konietzko-Meier and Sander, 2013; Sanchez and Schoch, 2013; McHugh, 2014; Canoville and Chinsamy, 2015; Teschner et al., 2018). This histodiversity partly results from a significant size variability and wide range of temnospondyl lifestyles (Schoch, 2009, 2014; Sanchez et al., 2010b). Indeed, the bone compactness (Laurin et al., 2004) and mass (de Ricqlès and de Buffrénil, 2001) often correlate with the lifestyle of tetrapods. The vascularization increases with the somatic size as a result of faster growth rate (de Buffrénil et al., 2008; Padian, 2012; Cubo et al., 2014; except for anurans, Canoville et al., 2018). Nevertheless, it seems that Paleozoic temnospondyls would tend to have a more constant pattern than the derived Mesozoic forms. Indeed many Triassic forms have a great ability to adapt different environments which gives rise to a great bone microstructural diversity (Sanchez and Schoch, 2013; Canoville and Chinsamy, 2015) that we consider as a derived character. Consequently, we decided to compare the limb bone histology of seymouriamorphs with that of Paleozoic temnospondyls of the same size – i.e., smaller than one meter long (tail included) – and whose lifestyles were amphibious to terrestrial. Only *Acheloma* (Dilkes and Reisz, 1987) and *Doleserpeton* (Sigurdsen and Bolt, 2010) are fully/partly terrestrial Paleozoic forms smaller than one meter and whose bone histology has been revealed. These taxa start forming periosteal bone in their humeri with a very simple primary bone organization made of a sublamellar to lamellar matrix (de Ricqlès, 1981; Sanchez et al., 2010b). Their

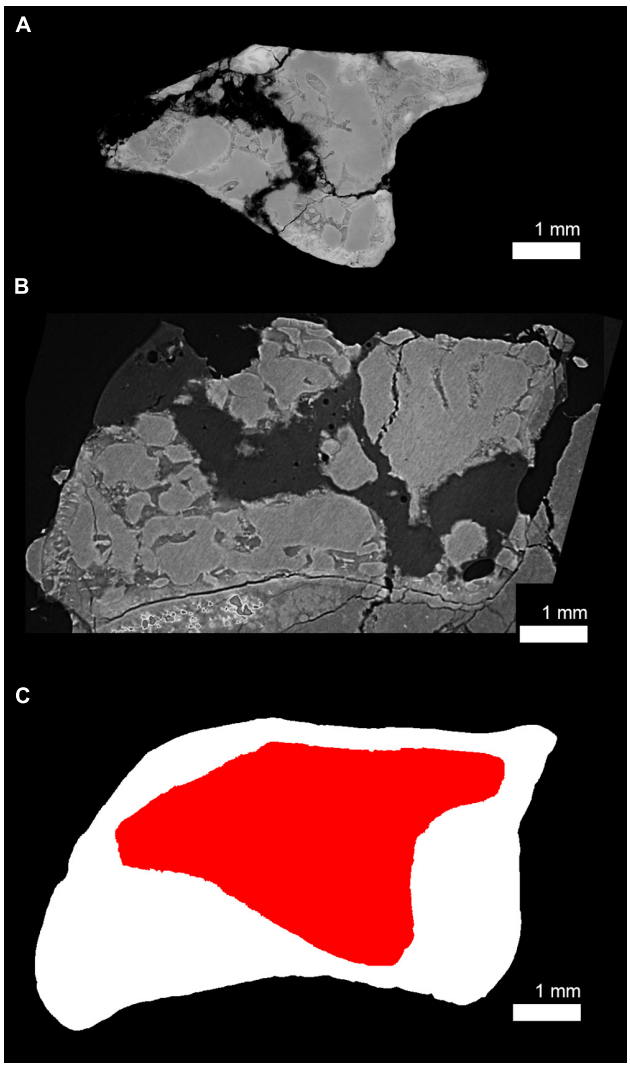

FIGURE 10 | Size differences between the juvenile (subadult) and adult humeral cross section of *Seymouria sanjuanensis*. **(A)** Virtual thin section of the juvenile humerus of *S. sanjuanensis* (MNG 7747, thickness: 40 μm) and **(B)** the adult humerus of *S. sanjuanensis* (CM 28597, thickness: 40 μm) at midshaft. Note that because the humerus of CM 28597 is a right humerus and that of MNG 7747 is a left one, the humerus of CM 28597 has been flipped for comparative purposes. **(C)** Overlap between the cross-sectional silhouettes of **(A)** (in red) and **(B)** (in white).

vascularization is primary, formed of small, scattered canals that seem more longitudinal than radial. The average bone deposition rate in the femur of *Doleserpeton* is of 36 μm between two LAGs (**Table 4**). This combination of features characterizes a slow bone deposition pace in adults which contrasts with the active bone dynamic deduced from the humeral histology of the adult *Seymouria* and the dense vascularity observed in the cortical core of *Discosauriscus* described in the current study. In terrestrial temnospondyls, erosion and remodeling occur secondarily to a moderate degree (de Ricqlès and de Buffrénil, 2001; Laurin et al., 2004). The innermost surface of the shaft of the femur of *Doleserpeton* exhibits a thin layer of endosteal bone after a slight erosion and *Acheloma* only restricts erosion to the innermost layer of the cortical bone (Sanchez et al., 2010b). This greatly diverges from the humeral cortex of the supposedly terrestrial *Seymouria* (Berman and Martens, 1993) whose total erosion of the innermost cortex tightly follows the bone deposition (**Figure 10**). Remodeling and erosion in the humerus of *Seymouria* therefore is an active process allowed by an active metabolism.

The humeral histology of extant salamanders (**Figure 1**) is often avascular and very poorly remodeled (e.g., Castanet et al., 2003; *Desmognathus*, Sanchez et al., 2012; Canoville et al., 2018) except for the larger species (Sanchez et al., 2014). For example, the giant salamander *Andrias* – which can reach between 1 and 2 m depending on the species – displays a primary bone pierced by canals. Nevertheless, these canals are small, anastomosed and remain primary despite an obvious although slight internal erosion in the innermost region of the cortex (Sanchez et al., 2014). These features clearly suggest a relatively slow bone deposition in the humerus of extant salamanders.

In this evolutionary context, the more densely vascularized humeral histology of seymouriamorphs, associated with a dense osteocytic population of rounded cells and, in *Seymouria*, a high degree of erosion, contrasts with other non-amniotic histological organizations observed in Devonian tetrapods, temnospondyls and extant salamanders. If seymouriamorphs are considered stem amniotes (based on the prevailing hypothesis, Milner, 1988; Trueb and Cloutier, 1991; Schoch and Milner, 2004; Ruta and Coates, 2007; Anderson, 2008; Sigurdsen and Green, 2011; Pardo et al., 2017a; Schoch, 2018), the bone histology of seymouriamorphs could indicate a first step toward a more active metabolism. If seymouriamorphs are considered stem tetrapods (Vallin and Laurin, 2004; Marjanović and Laurin, 2013), the histology of seymouriamorphs would reveal a unique increase of metabolic activity in the stem group of tetrapods.

Evolution of Growth Strategies in Early Tetrapods

Recently, several studies demonstrated that stem tetrapods had a relative long juvenile period before they could start reproducing. The tristichopterid *Eusthenopteron* could only reach adulthood after 10–11 years (Sanchez et al., 2014); and the early tetrapod *Acanthostega* had an extended pre-reproductive period lasting at least 6 years (Sanchez et al., 2016).

Paleozoic temnospondyls also seemed to acquire their sexual maturity relatively late. Although life-history traits tend to correlate with the size and body mass of species (Ricklefs, 2010), *Apateon* individuals – that were not more than 10 cm long – could extend their juvenile stage from 5 to 7 years (Sanchez et al., 2010a,b). In the limb-bone metaphysis of adult individuals of *Apateon*, the presence of remnants of uncalcified cartilage strongly supports the hypothesis of a relatively slow development (Sanchez et al., 2010a).

Once again, the Triassic forms of temnospondyls seem derived in that context too. *Gerrothorax* demonstrated a great variability of growth rates and life history traits subject to a broad

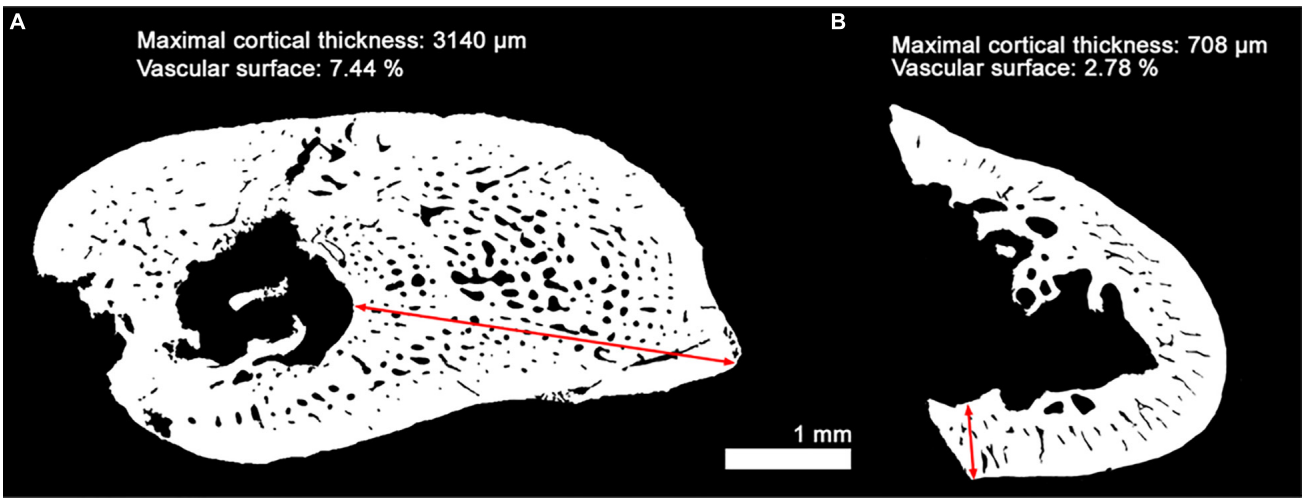

FIGURE 11 | Measurements of the cortical thickness and vascular surface in two different bones of the subadult *Discosauriscus austriacus* (SNM Z 15568). Comparison between two binary thin sections made in the humerus (current study; **A**) and the feur (Sanchez et al., 2008; **B**) of the subadult *D. austriacus* SNM Z 15568. The *vascular surface* values result from the ratio between the area covered by the vascularization over the area covered by the compact cortical bone. Red arrows show the maximal thickness of compact cortical tissue.

variation between specimens of different locations (Sanchez and Schoch, 2013). Some individuals of *Gerrothorax* could reach their sexual maturity much earlier (3–4 years) than others (6 years) (Sanchez and Schoch, 2013). The Triassic *Lydekkerina* exhibited as well a short juvenile stage (1 year, Canoville and Chinsamy, 2015). It was demonstrated that variability in life-history traits could be the essence for the survival of a taxon (González-Suárez and Revilla, 2013). On this basis, the Triassic forms, *Gerrothorax* and *Lydekkerina*, evolved to adjust their developmental strategy in relation with their extreme ecological conditions after the Permo-Triassic crisis. These environmental conditions greatly contrast with the Paleozoic (Carboniferous and Permian) conditions in which seymouriamorhs were living. For this reason, we decided once again to focus our comparisons on the Paleozoic forms of tetrapods only.

A skeletochronological analysis led by Sanchez et al. (2008) revealed that *Discosauriscus* took no less than 10 years to reach sexual maturity. However no LAGs could be observed in *Seymouria*'s limb bones, probably as a result of very active bone dynamics as demonstrated above. It seems that the only seymouriamorph whose life history could be revealed so far would tend to show a long pre-reproductive period. The shift toward an acceleration of the pre-reproductive period (exemplified by the Permian amniote *Ophiacodon* slowing down their skeletal development after 1 year; Laurin and de Buffrénil, 2016) would therefore tend to be a later event in the evolutionary history of amniotes. Nevertheless, nothing rules out that seymouriamorphs could display a large diversity in their reproductive strategy with *Seymouria* exhibiting a shorter pre-reproductive period. For this reason, life histories should be more broadly investigated within seymouriamorphs and other stem- or early- amniotes such as diadectids (Benson, 2012; Berman, 2013; Klembara et al., 2020).

CONCLUSION

Here we show that the seymouriamorphs *D. austriacus* and *S. sanjuanensis* developed relatively fast bone growth and dynamics (even though cyclically in the humerus of *D. austriacus*). This significantly contrasts with the slow primary bone deposit encountered in the stylopods of other non-amniotic Paleozoic tetrapods of equal sizes. However the seymouriamorph *D. austriacus* retains a long pre-reproductive period as observed in early tetrapods and Paleozoic temnospondyls. Because no growth marks could be observed in *S. sanjuanensis*, no inference can be made on their reproductive strategy. Nevertheless, this combination of features suggests that the amniotic developmental strategy probably did not occur as a drastic overall event but rather was a long-lasting process.

This study shows preliminary results as only based on the humeral histology of a few specimens of seymouriamorphs. More limb bones and more specimens of this group should be investigated to draw broad conclusions. In addition, other non-amniotic tetrapods and early amniotes (e.g., lepospondyls, diadectids) should be thoroughly investigated to characterize and date the acceleration of the pre-reproductive period as observed in small extant amniotes.

Not only the current study reveals new data on the limb bone histology of *S. sanjuanensis* but it also provides unprecedented 3D insights into the long bone of *D. austriacus* to adjust former interpretations. This illustrates the need to complement 2D cross-section observations on fossil material with 3D imaging in order to investigate the best-preserved museum-collection specimens usually unavailable to destructive techniques.

DATA AVAILABILITY STATEMENT

The datasets generated for this study can be found in the ESRF paleontological microtomographic database (http://paleo.esrf.eu).

AUTHOR CONTRIBUTIONS

SS and JE conceived the project, produced the figures, conducted the analyses and interpretations, and wrote the manuscript. JK conducted fieldwork and provided expertise on the seymouriamorphs. PT and SS generated the synchrotron data. PT reconstructed the scan data. JE segmented the scan data. SS provided the thin sections. All authors provided a critical review of the manuscript and approved the final draft.

FUNDING

Beamtime was allocated thanks to proposals accepted by the European Synchrotron Radiation Facility (EC203, SS) and inhouse beamtime. This research was supported by two grants from the Vetenskapsrådet (2015-04335 and 2019-04595, SS) and the Scientific Grant Agency of Ministry of Education of Slovak Republic and Slovak Academy of Sciences (1/0228/19, JK).

ACKNOWLEDGMENTS

We thank T. Hübner for access to the collections housed in the Museum der Natur of Gotha (Germany); D. Germain and A. de Ricqlès for access to the research collections of thin sections housed in the Muséum national d'Histoire naturelle of Paris (France); A. Durišová for access to the collections housed in the Slovak National Museum (Bratislava, Slovakia) and D. S. Berman and Amy C. Henrici for access to the collections of the Carnegie Museum of Natural History, Pittsburgh (United States). We want to thank the editorial board of Frontiers in Earth Science and more specifically M. Laurin who helped editing this article. Previous versions of this article were greatly improved thanks to the three reviewers and P. Ahlberg (Uppsala University).

SUPPLEMENTARY MATERIAL

The Supplementary Material for this article can be found online at: https://www.frontiersin.org/articles/10.3389/feart.2020.00097/full#supplementary-material

REFERENCES

Anderson, J. S. (2007). ""Incorporating ontogeny into the matrix: a phylogenetic evaluation of developmental evidence for the origin of modern amphibians"," in *Major Transitions in Vertebrate Evolution*, eds J. S. Anderson, and H.-D. Sues, (Bloomington: Indiana University Press), 182–227.

Anderson, J. S. (2008). Focal review: the origin(s) of modern amphibians. *Evol. Biol.* 35, 231–247. doi: 10.1007/s11692-008-9044-5

Benson, R. B. J. (2012). Interrelationships of basal synapsids: cranial and postcranial morphological partitions suggest different topologies. *J. Syst. Palaeonto.* 10, 601–624. doi: 10.1080/14772019.2011.631042

Berman, D. S. (1993). "Lower vertebrate localities of New Mexico and their assemblages," in *Vertebrate Paleontology in New Mexico*, Vol. 2, eds S. G. Lucas, and J. Zidek, (New Mexico: New Mexico Museum of Natural History and Science), 11–21.

Berman, D. S. (2013). "Diadectomorphs: amniotes or not?," in *The Carboniferous-Permian Transition*, Vol. 60, eds S. G. Lucas, W. A. DiMichele, J. E. Barrick, J. W. Schneider, and J. A. Spielmann, (New Mexico: New Mexico Museum of Natural History and Sciences), 22–35.

Berman, D. S., Henrici, A. C., Sumida, S. S., and Martens, T. (2000). Redescription of *Seymouria sanjuanensis* (*Seymouriamorpha*) from the lower permian of Germany based on complete, mature specimens with a discussion of paleoecology of the Bromacker locality assemblage. *J. Vertebr. Paleontol.* 20, 253–268. doi: 10.1671/0272-4634(2000)020%5B0253:rosssf%5D2.0.co;2

Berman, D. S., and Martens, T. (1993). First occurrence of *Seymouria* (*Amphibia*: *Batrachosauria*) in the lower permian rotliegend of central Germany. *Ann. Carnegie Mus.* 62, 63–79.

Berman, D. S., Reisz, R. R., and Eberth, D. A. (1987). *Seymouria sanjuanensis* (*Amphibia*, *Batrachosauria*) from the lower permian cutler formation of north-central New Mexico and the occurrence of sexual dimorphism in that genus questioned. *Can. J. Earth Sci.* 24, 1769–1784. doi: 10.1139/e87-169

Botha-Brink, J., and Modesto, S. P. (2007). A mixed-age classed 'pelycosaur' aggregation from South Africa: earliest evidence of parental care in amniotes? *Proc. R. Soc. B Bio. Sci.* 274, 2829–2834. doi: 10.1098/rspb.2007.0803

Bourdon, E., Castanet, J., de Ricqlès, A., Scofield, P., Tennyson, A., Lamrous, H., et al. (2009). Bone growth marks reveal protracted growth in New Zealand kiwi (Aves. *Apterygidae*). Biol. Lett. 5, 639–642. doi: 10.1098/rsbl.2009.0310

Canoville, A., and Chinsamy, A. (2015). Bone Microstructure of the Stereospondyl *Lydekkerina huxleyi* reveals adaptive strategies to the harsh post permian-extinction environment. *Anat. Record* 298, 1237–1254. doi: 10.1002/ar.23160

Canoville, A., Laurin, M., and de Buffrénil, V. (2018). Quantitative data on bone vascular supply in lissamphibians: comparative and phylogenetic aspects. *Zool. J. Linn. Soc.* 182, 107–128. doi: 10.1093/zoolinnean/zlx016

Castanet, J., Francillon-Vieillot, H., and de Ricqlès, A. (2003). "The skeletal histology of Amphibia," in *Amphibian Biology Vol. V- Osteology*, eds H. Heatwole, and M. Davies, (Chipping Norton: Surrey Beatty & Sons), 1598–1683.

Castanet, J., Francillon-Vieillot, H., Meunier, F.-J., and de Ricqlès, A. (1993). ""Bone and individual aging"," in *Bone Vol. 7: Bone Growth-B*, ed. B. K. Hall, (Boca Raton: CRC Press), 245–283.

Crump, M. L. (1996). ""Parental care among the amphibia"," in *Advances in the Study of Behavior*, Vol. 25, eds J. S. Rosenblatt, and C. T. Snowdon, (San Diego: Academic Press), 109–144. doi: 10.1016/s0065-3454(08)60331-9

Cubo, J., Baudin, J., Legendre, L., Quilhac, A., and de Buffrénil, V. (2014). Geometric and metabolic constraints on bone vascular supply in diapsids. *Biol. J. Linn. Soc.* 112, 668–677. doi: 10.1111/bij.12331

Cubo, J., and Casinos, A. (2000). Incidence and mechanical significance of pneumatization in the long bones of birds. *Zool. J. Linn. Soc.* 130, 499–510. doi: 10.1111/j.1096-3642.2000.tb02198.x

de Buffrénil, V., Houssaye, A., and Böhme, W. (2008). Bone vascular supply in monitor lizards (Squamata: Varanidae): influence of size, growth, and phylogeny. *J. Morphol.* 269, 533–543. doi: 10.1002/jmor.10604

de Margerie, E., Sanchez, S., Cubo, J., and Castanet, J. (2005). Torsional resistance as a principal component of the structural design of long bones: comparative multivariate evidence in birds. *Anat. Record Part A* 282, 49–66.

de Ricqlès, A. (1981). Recherches paléohistologiques sur les os longs des tétrapodes - VI. - *les stégocéphales*. *Ann. Paléontol.* 67, 141–157.

de Ricqlès, A., and de Buffrénil, V. (2001). "Bone histology, heterochronies and the return of tetrapods to life in water: where are we," in *Secondary Adaptation of Tetrapods to Life in Water*, eds J.-M. Mazin, and V. de Buffrénil, (München: Verlag Dr. Friedrich Pfeil), 289–310.

de Ricqlès, A., Horner, J. R., and Padian, K. (2006). The interpretation of dinosaur growth patterns. *Science* 21, 596–597. doi: 10.1016/j.tree.2006.08.005

de Ricqlès, A. (1979). Relations entre structures histologiques, ontogenèse, stratégies démographiques et modalités évolutives: le cas des reptiles captorhinomorphes et des stégocéphales temnospondyles. *Compt. Sci., Paris* 288, 1147–1150.

Dilkes, D. W., and Reisz, R. R. (1987). *Trematops milleri* Williston, 1909 identified as a junior synonym of *Acheloma cumminsi* Cope, 1882, with a revision of the genus. *Am. Mus. Novit.* 2902, 1–12.

Duellman, W. E., and Trueb, L. (1994). *Biology of Amphibians*. Baltimore: JHU press.

Erickson, G. M. (2005). Assessing dinosaur growth patterns: a microscopic revolution. *Trends Ecol. Evol.* 20, 677–684. doi: 10.1016/j.tree.2005.08.012

Francillon-Vieillot, H., de Buffrénil, V., Castanet, J., Géraudie, J., Meunier, F.-J., Sire, J.-Y., et al. (1990). "Microstructure and mineralization of vertebrate skeletal tissues," in *Skeletal Biomineralization: Patterns, Processes and Evolutionary Trends*, (New York, NY: Van Nostrand Reinhold), 471–530. doi: 10.1007/978-1-4899-5740-5_20

Girondot, M., and Laurin, M. (2003). Bone profiler: a tool to quantify, model, and statistically compare bone-section compactness profiles. *J. Vertebr. Paleontol.* 23, 458–461. doi: 10.1671/0272-4634(2003)023[0458:bpattq]2.0.co;2

González-Suárez, M., and Revilla, E. (2013). Variability in life-history and ecological traits is a buffer against extinction in mammals. *Ecol. Lett.* 16, 242–251. doi: 10.1111/ele.12035

Kamska, V., Daeschler, E. B., Downs, J. P., Ahlberg, P. E., Tafforeau, P., and Sanchez, S. (2019). Long-bone development and life-history traits of the devonian tristichopterid *Hyneria lindae*. *Earth Environ. Sci. Trans. R. Soc. Edinb.* 109, 75–86. doi: 10.1017/s175569101800083x

Klembara, J. (1995). The external gills and ornamentation of skull roof bones of the Lower Permian tetrapod *Discosauriscus* (Kuhn 1933) with remarks to its ontogeny. *Paläontol. Z.* 69, 265–281. doi: 10.1007/bf02985990

Klembara, J. (2009). New cranial and dental features of *Discosauriscus austriacus* (Seymouriamorpha, Discosauriscidae) and the ontogenetic conditions of *Discosauriscus*. *Special Pap. Palaeontol.* 81, 61–69.

Klembara, J., and Bartík, I. (1999). The postcranial skeleton of *Discosauriscus* Kuhn, a seymouriamorph tetrapod from the lower permian of the Boskovice Furrow (Czech Republic). *Trans. R. Soc. Edinb.* 90, 287–316. doi: 10.1017/s0263593300002649

Klembara, J., Berman, D. S., Henrici, A. C., Ceròanskı, A., and Werneburg, R. (2006). Comparison of cranial anatomy and proportions of similarly sized *Seymouria sanjuanensis* and *Discosauriscus austriacus*. *Ann. Carnegie Mus.* 75, 37–49. doi: 10.2992/0097-4463(2006)75[37:cocaap]2.0.co;2

Klembara, J., Berman, D. S., Henrici, A. C., Èeròanskı, A., Werneburg, R., and Martens, T. (2007). First description of skull of lower permian *Seymouria sanjuanensis* (*Seymouriamorpha*: *Seymouriidae*) at an early juvenile stage. *Ann. Carnegie Mus.* 76, 53–72. doi: 10.2992/0097-4463(2007)76[53:fdosol]2.0.co;2

Klembara, J., Clack, J. A., Milner, A. R., and Ruta, M. (2014). Cranial anatomy, ontogeny, and relationships of the Late Carboniferous tetrapod *Gephyrostegus bohemicus* Jaekel, 1902. *J. Vertebr. Paleontol.* 34, 774–792. doi: 10.1080/02724634.2014.837055

Klembara, J., Hain, M., Ruta, M., Berman, D. S., Pierce, S. E., and Henrici, A. C. (2020). Inner ear morphology of diadectomorphs and seymouriamorphs (Tetrapoda) uncovered by high-resolution X-ray microcomputed tomography, and the origin of the amniote crown group. *Palaeontology* 63, 131–154. doi: 10.1111/pala.12448

Klembara, J., Martens, T., and Bartík, I. (2001). The postcranial remains of a juvenile seymouriamorph tetrapod from the lower permian rotliegend of the tambach formation of central Germany. *J. Vertebr. Paleontol.* 21, 521–527. doi: 10.1671/0272-4634(2001)021[0521:tproaj]2.0.co;2

Klembara, J., and Meszároš, S. (1992). New finds of *Discosauriscus austriacus* (Makowsky 1876) from the Lower Permian of Boskovice Furrow (Czecho-Slovakia). *Geol. Carpath.* 43, 305–312.

Köhler, M., Marín-Moratalla, N., Jordana, X., and Aanes, R. (2012). Seasonal bone growth and physiology in endotherms shed light on dinosaur physiology. *Nature* 487, 358–361. doi: 10.1038/nature11264

Konietzko-Meier, D., and Klein, N. (2013). Unique growth pattern of *Metoposaurus diagnosticus krasiejowensis* (*Amphibia*, *Temnospondyli*) from the Upper Triassic of Krasiejów, Poland. *Palaeogeogr. Palaeoclimatol. Palaeoecol.* 370, 145–157. doi: 10.1016/j.palaeo.2012.12.003

Konietzko-Meier, D., and Sander, P. M. (2013). Long bone histology of *Metoposaurus diagnosticus* (*Temnospondyli*) from the late triassic of Krasiejów (Poland) and its paleobiological implications. *J. Vertebr. Paleontol.* 33, 1003–1018. doi: 10.1080/02724634.2013.765886

Kriloff, A., Germain, D., Canoville, A., Vincent, P., Sache, M., and Laurin, M. (2008). Evolution of bone microanatomy of the tetrapod tibia and its use in palaeobiological inference. *J. Evol. Biol.* 21, 807–826. doi: 10.1111/j.1420-9101.2008.01512.x

Labiche, J. C., Mathon, O., Pascarelli, S., Newton, M. A., Guilera Ferre, G., Curfs, C., et al. (2007). The fast readout low noise camera as a versatile x-ray detector for time resolved dispersive extended x-ray absorption fine structure and diffraction studies of dynamic problems in materials science, chemistry, and catalysis. *Rev. Sci. Instrum.* 78:091301. doi: 10.1063/1.2783112

Laurin, M., and de Buffrénil, V. (2016). Microstructural features of the femur in early ophiacodontids: a reappraisal of ancestral habitat use and lifestyle of amniotes. *C. R. Palevol.* 15, 115–127. doi: 10.1016/j.crpv.2015.01.001

Laurin, M., Germain, D., Steyer, J.-S., and Girondot, M. (2006). Données microanatomiques sur la conquête de l'environnement terrestre par les vertébrés. *C. R. Palevol* 5, 603–618. doi: 10.1016/j.crpv.2005.09.023

Laurin, M., Girondot, M., and Loth, M.-M. (2004). The evolution of long bone microstructure and lifestyle in lissamphibians. *Paleobiology* 30, 589–613. doi: 10.1666/0094-8373(2004)030<0589:teolbm>2.0.co;2

Marjanović, D., and Laurin, M. (2013). The origin(s) of extant amphibians: a review with emphasis on the "lepospondyl hypothesis". *Geodiversitas* 35, 207–272.

McHugh, J. B. (2014). Paleohistology and histovariability of the Permian stereospondyl *Rhinesuchus*. *J. Vertebr. Paleontol.* 34, 59–68. doi: 10.1080/02724634.2013.787429

Milner, A. R. (1988). "The relationships and origin of living amphibians," in *The Phylogeny and Classification of the Tetrapods*, ed. M. Benton, (Oxford: Clarendon Press), 59–102.

Mirone, A., Brun, E., Gouillart, E., Tafforeau, P., and Kieffer, J. (2014). The PyHST2 hybrid distributed code for high speed tomographic reconstruction with iterative reconstruction and a priori knowledge capabilities. *Nucl. Instrum. Methods Phys. Res. Section B Beam Interactions Mater. Atoms* 324, 41–48. doi: 10.1016/j.nimb.2013.09.030

Mukherjee, D., Ray, S., and Sengupta, D. P. (2010). Preliminary observations on the bone microstructure, growth patterns, and life habits of some Triassic temnospondyls from India. *J. Vertebr. Paleonto.* 30, 78–93. doi: 10.1080/02724630903409121

Padian, K. (2012). Evolutionary physiology: a bone for all seasons. *Nature* 487, 310–311. doi: 10.1038/nature11382

Padian, K., de Ricqlès, A. J., and Horner, J. R. (2001). Dinosaurian growth rates and bird origins. *Nature* 412, 405–408. doi: 10.1038/35086500

Paganin, D., Mayo, S. C., Gureyev, T. E., Miller, P. R., and Wilkins, S. W. (2002). Simultaneous phase and amplitude extraction from a single defocused image of a homogeneous object. *J. Microsc.* 206, 33–40. doi: 10.1046/j.1365-2818.2002.01010.x

Pardo, J. D., Small, B. J., and Huttenlocker, A. K. (2017a). Stem caecilian from the Triassic of Colorado sheds light on the origins of *Lissamphibia*. *Proc. Natl. Acad. Sci.U.S.A.* 114, E5389–E5395.

Pardo, J. D., Szostakiwskyj, M., Ahlberg, P. E., and Anderson, J. S. (2017b). Hidden morphological diversity among early tetrapods. *Nature* 546, 642–645. doi: 10.1038/nature22966

Piñeiro, G., Ferigolo, J., Meneghel, M., and Laurin, M. (2012). The oldest known amniotic embryos suggest viviparity in mesosaurs. *Histor. Biol.* 24, 620–630. doi: 10.1080/08912963.2012.662230

Rafferty, A. R., and Reina, R. D. (2012). Arrested embryonic development: A review of strategies to delay hatching in egg-laying reptiles. *Proc. R. Soc. B Biol. Sci.* 279, 2299–2308. doi: 10.1098/rspb.2012.0100

Reisz, R. R. (1997). The origin and early evolutionary history of amniotes. *Trends Ecol. Evol.* 12, 218–222. doi: 10.1016/s0169-5347(97)01060-4

Ricklefs, R. E. (2010). Life-history connections to rates of aging in terrestrial vertebrates. *Proc. Natl. Acad. Sci.U.S.A.* 107, 10314–10319. doi: 10.1073/pnas.1005862107

Romer, A. S. (1928). A skeletal model of the primitive reptile *Seymouria*, and the phylogenetic position of that type. *J. Geol.* 36, 248–260. doi: 10.1086/623510

Ruta, M., and Coates, M. I. (2007). Dates, nodes and character conflict: addressing the lissamphibian origin problem. *J. Syst. Palaeontol.* 5, 69–122. doi: 10.1017/s1477201906002008

Ruta, M., Pisani, D., Lloyd, G. T., and Benton, M. J. (2007). A supertree of *Temnospondyli*: cladogenetic patterns in the most species-rich group of early tetrapods. *Proc. R. Soc. B Biol. Sci.* 274, 3087–3095. doi: 10.1098/rspb.2007.1250

San Mauro, D. (2010). A multilocus timescale for the origin of extant amphibians. *Mol. Phylogenet. Evol.* 56, 554–561. doi: 10.1016/j.ympev.2010.04.019

Sanchez, S., Ahlberg, P. E., Trinajstic, K. M., Mirone, A., and Tafforeau, P. (2012). Three-dimensional synchrotron virtual paleohistology: a new insight into the world of fossil bone microstructures. *Microsc. Microanal.* 18, 1095–1105. doi: 10.1017/s1431927612001079

Sanchez, S., de Ricqlès, A., Schoch, R. R., and Steyer, J.-S. (2010a). Developmental plasticity of limb bone microstructural organization in *Apateon*: histological evidence of paedomorphic conditions in branchiosaurs. *Evol. Dev.* 12, 315–328. doi: 10.1111/j.1525-142x.2010.00417.x

Sanchez, S., Germain, D., de Ricqlès, A., Abourachid, A., Goussard, F., and Tafforeau, P. (2010b). Limb-bone histology of temnospondyls: implications for understanding the diversification of palaeoecologies and patterns of locomotion of Permo-Triassic tetrapods. *J. Evol. Biol.* 23, 2076–2090. doi: 10.1111/j.1420-9101.2010.02081.x

Sanchez, S., Dupret, V., Tafforeau, P., Trinajstic, K., Ryll, B., Gouttenoire, P.-J., et al. (2013). 3D microstructural architecture of muscle attachments in extant and fossil vertebrates revealed by synchrotron microtomography. *Plos One* 8, e56992. doi: 10.1371/journal.pone.0056992

Sanchez, S., Klembara, J., Castanet, J., and Steyer, J.-S. S. (2008). Salamander-like development in a seymouriamorph revealed by palaeohistology. *Biol. Lett.* 4, 411–414. doi: 10.1098/rsbl.2008.0159

Sanchez, S., and Schoch, R. R. (2013). Bone histology reveals a high environmental and metabolic plasticity as a successful evolutionary strategy in a long-lived homeostatic Triassic temnospondyl. *Evol. Biol.* 40, 627–647. doi: 10.1007/s11692-013-9238-3

Sanchez, S., Tafforeau, P., and Ahlberg, P. E. (2014). The humerus of *Eusthenopteron*: a puzzling organization presaging the establishment of tetrapod limb bone marrow. *Proc. R. Soc. Lon. B* 281:20140299. doi: 10.1098/rspb.2014.0299

Sanchez, S., Tafforeau, P., Clack, J. A., and Ahlberg, P. E. (2016). Life history of the stem tetrapod *Acanthostega* revealed by synchrotron microtomography. *Nature* 537, 408–411. doi: 10.1038/nature19354

Sander, P. M. (2012). Reproduction in early amniotes. *Science* 337, 806–808. doi: 10.1126/science.1224301

Sander, P. M., Klein, N., Buffetaut, E., Cuny, G., Suteethorn, V., and Le Loeuff, J. (2004). Adaptative radiation in sauropod dinosaurs: bone histology indicates rapid evolution of giant body size through acceleration. *Org. Divers. Evol.* 4, 165–173. doi: 10.1016/j.ode.2003.12.002

Schoch, R., and Milner, A. R. (2004). "Structure and implications of the theories on the origin of lissamphibians," in *Recent Advances in the Origin and Early Radiation of Vertebrates*, eds G. Arratia, M. V. H. Wilson, and R. Cloutier, (München: Verlag Dr. Friedrich Pfeil), 345–376.

Schoch, R. R. (2009). Evolution of life cycles in early amphibians. *Annu. Rev. Earth Planet. Sci.* 37, 135–162. doi: 10.1146/annurev.earth.031208.100113

Schoch, R. R. (2014). Life cycles, plasticity and palaeoecology in temnospondyl amphibians. *Palaeontology* 57, 517–529. doi: 10.1111/pala.12100

Schoch, R. R. (2018). Osteology of the temnospondyl *Neldasaurus* and the evolution of basal dvinosaurians. *Neues Jahrb. Geol. Paläontol. Abh.* 287, 1–16. doi: 10.1127/njgpa/2018/0700

Sigurdsen, T., and Bolt, J. R. (2010). The lower permian amphibamid *Doleserpeton* (*Temnospondyli*: *Dissorophoidea*), the interrelationships of amphibamids, and the origin of modern amphibians. *J. Vertebr. Paleontol.* 30, 1360–1377. doi: 10.1080/02724634.2010.501445

Sigurdsen, T., and Green, D. M. (2011). The origin of modern amphibians: a re-evaluation. *Zool. J. Linn. Soc.* 162, 457–469. doi: 10.1111/j.1096-3642.2010.00683.x

Steyer, J.-S., Laurin, M., Castanet, J., and de Ricqlès, A. (2004). First histological and skeletochronological data on temnospondyl growth: palaeoecological and palaeoclimatological implications. *Palaeogeogr. Palaeoclimatol.Palaeoecol.* 206, 193–201. doi: 10.1016/j.palaeo.2004.01.003

Sumida, S. S., and Martin, K. L. M. (1997). *Amniote Origins*. San Diego: Academic Press.

Tafforeau, P., Bentaleb, I., Jaeger, J., and Martin, C. (2007). Nature of laminations and mineralization in rhinoceros enamel using histology and X-ray synchrotron microtomography: potential implications for palaeoenvironmental isotopic studies. *Palaeogeogr. Palaeoclimatol. Palaeoecol.* 246, 206–227. doi: 10.1016/j.palaeo.2006.10.001

Tafforeau, P., Boistel, R., Boller, E., Bravin, A., Brunet, M., Chaimanee, Y., et al. (2006). Applications of X-ray synchrotron microtomography for non-destructive 3D studies of paleontological specimens. *Appl. Phys. A* 83, 195–202. doi: 10.1007/s00339-006-3507-2

Tafforeau, P., and Smith, T. M. (2008). Nondestructive imaging of hominoid dental microstructure using phase contrast X-ray synchrotron microtomography. *J. Hum. Evol.* 54, 272–278. doi: 10.1016/j.jhevol.2007.09.018

Tafforeau, P., Zermeno, J. P., and Smith, T. M. (2012). Tracking cellular-level enamel growth and structure in 4D with synchrotron imaging. *J. Hum. Evol.* 62, 424–428. doi: 10.1016/j.jhevol.2012.01.001

Teschner, E. M., Sander, P. M., and Konietzko-Meier, D. (2018). Variability of growth pattern observed in *Metoposaurus krasiejowensis* humeri and its biological meaning. *J. Iberian Geol.* 44, 99–111. doi: 10.1007/s41513-017-0038-y

Trueb, L., and Cloutier, R. (1991). ""A phylogenetic investigation of the inter- and intrarelationships of the Lissamphibia (*Amphibia*: *Temnospondyli*)"," in *Origins of the Higher Groups of Tetrapods: Controversy and Consensus*, eds H.-P. Schultze, and L. Trueb, (New York, NY: Cornell university Press), 223–313.

Vallin, G., and Laurin, M. (2004). Cranial morphology and affinities of *Microbrachis*, and a reappraisal of the phylogeny and lifestyle of the first amphibians. *J. Vertebr. Paleontol.* 24, 56–72. doi: 10.1671/5.1

van Soest, R. W. M., and van Utrecht, W. L. (1971). The layered structure of bones of birds as a possible indication of age. *Bijdragen tot de Dierkunde* 41, 61–66. doi: 10.1163/26660644-04101008

Vaughn, P. P. (1966). *Seymouria* from the lower Permian of southeastern Utah, and possible sexual dimorphism in that genus. *J. Paleontol.* 40, 603–612.

White, T. (1939). Osteology of *Seymouria baylorensis* Broili. *Bull. Mus. Comp. Zool. Harvard Coll.* 85, 325–409.

Witzmann, F. (2009). Comparative histology of sculptured dermal bones in basal tetrapods, and the implications for the soft tissue dermis. *Palaeodiversity* 2, 233–270.

Woodward, H. N., Horner, J. R., and Farlow, J. O. (2014). Quantification of intraskeletal histovariability in *Alligator mississippiensis* and implications for vertebrate osteohistology. *PeerJ* 2:e422. doi: 10.7717/peerj.422

Conflict of Interest: The authors declare that the research was conducted in the absence of any commercial or financial relationships that could be construed as a potential conflict of interest.